Department of Physics and Astronomy
University of Heidelberg

Bachelor Thesis in Physics
submitted by

Cakir, Halil

born in Mannheim (Germany)

2013

Precise Determination of the $c\bar{c}$ Cross Section in proton-proton Collisions at $\sqrt{s} = 7\,\mathrm{TeV}$

Abstract

The cross sections of the charmed hadrons D^0, D^+, D^{*+}, D_s^+ and Λ_c^+ have been extrapolated over the full phase space using measurements of ALICE and LHCb at LHC covering a large region of the phase, namely $|y| < 0.5$ for ALICE and $2.0 < y < 4.5$ for LHCb, by using theoretical predictions obtained from the FONLL calculation framework and the PYTHIA 8.175 event generator. The FONLL and PYTHIA predictions have been compared to the experimental data. We observed that the shape of the measured p_{T}-distributions is well described by these predictions. We determined the total charm pair cross section in proton-proton collisions at $\sqrt{s} = 7\,\mathrm{TeV}$ as

$$\sigma_{\mathrm{tot}}(c\bar{c}) = 7.13 \pm 0.14\ (\mathrm{stat})^{+0.33}_{-0.43}\ (\mathrm{syst}) \pm 0.13\ (\mathrm{lum}) \pm 0.24\ (\mathrm{BR})^{+0.35}_{-0.12}\ (\mathrm{extr})\,\mathrm{mb}\ ,$$

$$\sigma_{\mathrm{tot}}(c\bar{c}) = 7.13^{+0.57}_{-0.54}\ (\mathrm{total})\,\mathrm{mb}\ .$$

This is the most precise determination of the charm pair cross section at the LHC to date.

Kurzdarstellung

Die Wirkungsquerschnitte der Charm-Hadronen D^0, D^+, D^{*+}, D_s^+ und Λ_c^+ wurden anhand von Messungen von ALICE und LHCb am LHC extrapoliert. Zu diesem Zweck wurden perturbative QCD Rechnungen mit FONLL und Ergebnisse vom Ereignisgenerator PYTHIA 8.175 verwendet. Die FONLL und PYTHIA Rechnungen wurden mit experimentellen Daten verglichen. Wir konnten feststellen, dass die Vorhersagen den Verlauf der gemessenen p_{T}-Distributionen korrekt beschreiben. Wir haben den totalen Charm-Paar Wirkungsquerschnitt in Proton-Proton Kollisionen für $\sqrt{s} = 7\,\mathrm{TeV}$ ermittelt. Unser Ergebnis lautet

$$\sigma_{\mathrm{tot}}(c\bar{c}) = 7.13 \pm 0.14\ (\mathrm{stat})^{+0.33}_{-0.43}\ (\mathrm{syst}) \pm 0.13\ (\mathrm{lum}) \pm 0.24\ (\mathrm{BR})^{+0.35}_{-0.12}\ (\mathrm{extr})\,\mathrm{mb}\ ,$$

$$\sigma_{\mathrm{tot}}(c\bar{c}) = 7.13^{+0.57}_{-0.54}\ (\mathrm{total})\,\mathrm{mb}\ .$$

Dies ist die bislang genaueste Bestimmung des Charm-Paar Wirkungsquerschnittes am LHC.

This Bachelor Thesis has been carried out by Halil Cakir at the
Physikalisches Institut in Heidelberg
under the supervision of
Dr. Kai Schweda

Contents

1 Introduction

Measurements of charm production in proton-proton collisions test predictions of perturbative Quantum Chromodynamics (QCD). Further, the charm pair cross section is an important parameter in statistical calculations of charmed hadron production in high-energy nucleus-nucleus collisions [1], [2]. The ATLAS, ALICE and LHCb collaborations at the Large Hadron Collider (LHC) have measured charm production in proton-proton collisions at $\sqrt{s} = 7\,\text{TeV}$ by measuring charmed hadron cross sections, since charm quarks hadronize soon after their production and thus cannot be detected directly. The measurements are provided in ref. [3], [4], [5] and [6]. However, due to experimental limitations, these cross sections could only be measured in a restricted range of transverse momentum p_T and rapidity y. Recently, LHCb published cross sections for D mesons D^0, D^+, D^{*+}, D_s^+ and for the charmed baryon Λ_c^+ measured in the forward rapidity range $2.0 < y < 4.5$ [6]. ALICE already measured cross sections for the D mesons at mid-rapidity $|y| < 0.5$. Both experiments extrapolated the total charm cross section from their own measurements. However, these extrapolated cross sections had large uncertainties mainly originating from the extrapolation. An important observation is, that ALICE and LHCb already cover a large domain of the (p_T, y) phase space. Since most charm quarks are produced at low rapidities, combining the measurements of ALICE and LHCb and performing an extrapolation using this combination should reduce uncertainties related to the extrapolation since the measurements cover a large region of the phase space.

The aim of this thesis is to extrapolate the charm pair cross section using the combined results of ALICE and LHCb. This thesis is organized as follows: In section 2 we will give a general explanation of the theory behind heavy quark production in hadron-hadron collisions. In section 3 we will introduce the FONLL calculation framework, which we will use to obtain theoretical predictions for the D meson cross sections. This is followed by section 4 where we will discuss the combination of the ALICE and LHCb measurements and explain how the cross sections of charmed hadrons and of charm pairs have been extrapolated. Finally, in the last section 5 we will summarize our results.

Note that within this thesis we used natural units, i.e. $\hbar = c = 1$. Plots shown in this thesis have been produced mainly with Matplotlib [7].

2 Heavy Quark Production in Hadron-Hadron Collisions

Charm, bottom and top quarks are considered to be heavy quarks due to their large masses. The heavy quark production in the collision of two hadrons H_1 and H_2 is given by the reaction

$$H_1 + H_2 \longrightarrow Q + \bar{Q} + X \ , \tag{2.1}$$

where Q denotes the heavy quark and $\bar{Q}$ the corresponding anti-quark. Due to confinement, quarks cannot be observed freely. They are bound in color-neutral hadrons. Therefore, soon after their production, the heavy quark pairs hadronize and form hadrons. In this section we will explain the theoretical basis of this process step by step.

2.1 Renormalization and asymptotic freedom

In calculations of probability amplitudes in the context of quantum field theories, it is possible that the involved integrals are divergent and therefore ill-defined. One possibility for a process involving divergent terms is illustrated in figure 2.1. Loops like in this figure

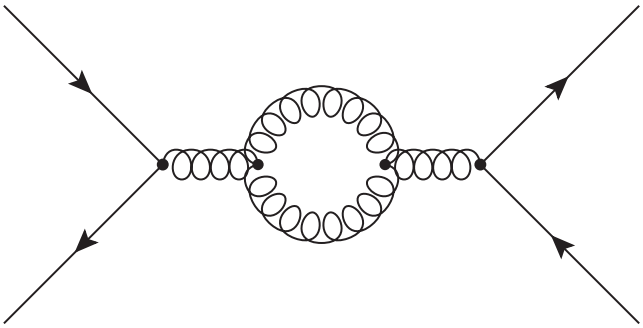

Figure 2.1: An example for a Feynman diagram with a loop. Such loops are related to effects on a very short time scale.

give rise to so-called ultraviolet divergences which are related to very short time or very high energy scales respectively. In order to account for these ultraviolet divergences in our calculations, we have to redefine free parameters of the theory like the mass or the coupling constant absorbing divergent terms. This procedure is called renormalization and the quantities we obtain are renormalized ones. The dependence of the renormalized quantities on the so-called renormalization scale μ_R is then given by the renormalization

group equations (RGE) of the underlying quantum field theory. For instance, the scale dependence of the strong coupling constant α_S is determined by the RGE

$$\mu_R^2 \frac{\mathrm{d}\alpha_S(\mu_R^2)}{\mathrm{d}(\mu_R^2)} = \beta(\alpha_S(\mu_R^2)) \,, \tag{2.2}$$

with the beta-function $\beta(\alpha_S(\mu_R^2))$. Equation 2.2 is an ordinary differential equation of first order, which can be integrated for a given boundary condition $\alpha_S(\mu_0^2)$ at some scale μ_0. The leading order approximation of the differential equation 2.2 is given by

$$\mu_R^2 \frac{\mathrm{d}\alpha_S(\mu_R^2)}{\mathrm{d}(\mu_R^2)} = -\frac{\beta_0}{12\pi}\alpha_S^2(\mu_R^2) \,, \tag{2.3}$$

where $\beta_0 = 33 - 2N_f$ and N_f denotes the number of active quark flavours. This leading order approximation has the solution

$$\alpha_S(\mu_R^2) = \frac{\alpha_S(\mu_0^2)}{1 + \frac{\beta_0}{12\pi}\alpha_S(\mu_0^2)\log(\mu_R^2/\mu_0^2)} \tag{2.4}$$

for a given value $\alpha_S(\mu_0^2)$. So, one can measure the strong coupling at some initial scale μ_0 and then determine the scale dependence using the renormalization group equations. Typically, one choses the strong coupling constant at $\mu_0 = M_Z$ as boundary condition, where $M_Z = 91.1876 \pm 0.0021\,\mathrm{GeV}$ [8] denotes the mass of the Z-boson. Then, we have $\alpha_S(M_Z^2) = 0.1184 \pm 0.0007$ as the world average cited by [8]. We can write the strong coupling constant as a function of the scale in the more convenient form

$$\alpha_S(\mu_R^2) = \frac{12\pi}{\beta_0 \log(\mu_R^2/\Lambda^2)} \,, \tag{2.5}$$

where $\Lambda = \mu_0^2 \exp(-12\pi/(\beta_0\alpha_S(\mu_0^2))) \approx 0.2\,\mathrm{GeV}$ is defining the scale at which the strong coupling $\alpha_S(\mu_R^2)$ diverges. Considering equation 2.5, we observe that the strong coupling decreases as the renormalization scale μ_R increases. This means that the interaction is strong at low but weak at high energy scales. This important property of the strong coupling α_S is called asymptotic freedom and has a central role in perturbative calculations. For energy scales smaller than Λ the strong coupling α_S is large and therefore perturbative calculations are not amenable. However, for energy scales much higher than Λ, α_S is small and therefore perturbative calculations are possible. Since Λ defines the border between perturbative and non-perturbative scales, it is called the non-perturbative scale of QCD.

Recall that the dependency of the strong coupling constant on the renormalization scale had been introduced to take care of ultraviolet divergences and has no physical justification. Therefore, a physical observable A has to be independent of the renormalization scale. That is, the observable A satisfies

$$\mu_R^2 \frac{\mathrm{d}A(\mu_R^2)}{\mathrm{d}(\mu_R^2)} = 0 \,. \tag{2.6}$$

In practice, one considers the perturbative expansion of A up to some finite order. Thus, there is still a residual dependence on the renormalization scale since full calculations of the expansion are often not possible. In order to estimate the dependence on the renormalization scale, the scale is varied in a certain range and the corresponding variation of the observable A is taken as an uncertainty due to scale dependence.

2.2 Factorization

Since we have hadrons in the initial state of the collision process, low energy scales due to the confinement of color-charge are inevitable. Thus, the strong coupling constant is large and a perturbative approach is not possible. However, we can use the factorization theorem of QCD [9] to separate soft processes, which are of non-perturbative nature, from hard processes, which are amenable to perturbation theory.

Another problem is that higher order Feynman diagrams include so-called infrared and collinear singularities. Infrared singularities are caused by the radiation and the exchange of gluons with low momentum. Collinear singularities originate from the emission of gluons collinear with the emitting particle. Whereas ultraviolet singularities are related to very short time scales, infrared and collinear singularities are related to very long time scales and thus small energy scales.

To attack these two problems, we depict a hadron in the initial state as a composition of pointlike constituents called *partons*. We can view the term parton as an umbrella term for quarks and gluons. The notion of factorization is then illustrated in figure 2.2.

The differential cross section for heavy quark production in hadron-hadron collisions is given by

$$\mathrm{d}\sigma_{H_1H_2}^{Q\bar{Q}X} = \sum_{i,j} \int \mathrm{d}x_1 \int \mathrm{d}x_2 \, F_{H_1}^i(x_1, \mu_F^2) F_{H_2}^j(x_2, \mu_F^2) \, \mathrm{d}\hat{\sigma}_{ij}^{Q\bar{Q}X}(p_1, p_2, \mu_R^2, \mu_F^2) \,. \tag{2.7}$$

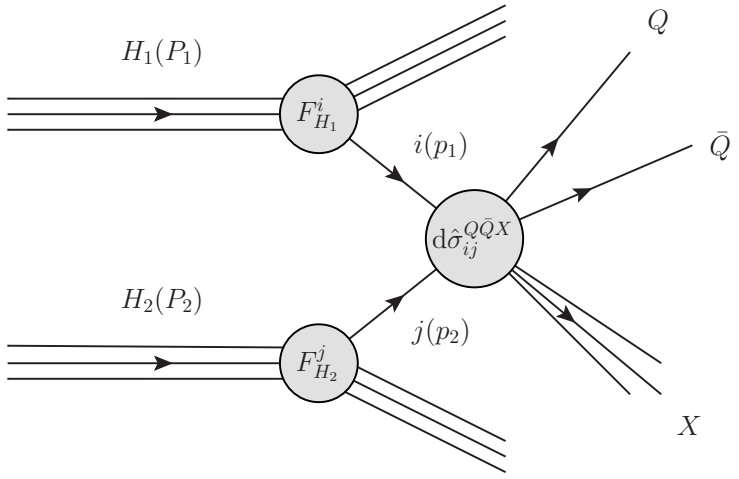

Figure 2.2: The factorized picture of heavy quark production in hadron-hadron collisions. H_1 and H_2 denote the colliding hadrons with four-momenta P_1 and P_2 respectively. $F^i_{H_1}$ and $F^j_{H_2}$ are the parton distribution functions, i and j are the interacting partons with four-momenta p_1 and p_2. The hard scattering cross section $\mathrm{d}\hat{\sigma}^{Q\bar{Q}X}_{ij}$ describes the probability to produce a heavy quark pair $Q\bar{Q}$ in the interaction of the partons i and j.

If P_1 and P_2 are the (four-)momenta of the incoming hadrons H_1 and H_2 respectively, then x_1 and x_2 denote the momentum fractions of the hadrons momentum carried by the interacting partons i and j. That is, for the momenta of the interacting partons p_1 and p_2 we have $p_1 = x_1 P_1$ and $p_2 = x_2 P_2$. The functions $F^i_{H_1}(x_1, \mu_F^2)$ and $F^j_{H_2}(x_2, \mu_F^2)$ are the parton distribution functions of the colliding hadrons H_1 and H_2. For example, $F^i_{H_1}(x_1, \mu_F^2)$ describes the probability density for finding a parton i, which carries the momentum fraction x_1 of the hadron, inside the hadron H_1. Besides the dependence on the momentum fraction of the parton, the parton distribution functions also depend on the so-called factorization scale μ_F. As in the renormalization procedure, this scale dependence is introduced to conceal divergences due to very low energy scales, as described above, in the parton distribution function. The evolution of the distribution functions as a function of the scale is then determined by the DGLAP[1] equation. That is, once you measured the parton distribution function for a given momentum fraction and factorization scale, you can evolve it to any scale using the DGLAP equation. However, the renormalization and factorization scales μ_R and μ_F are artificial parameters to avoid divergences. Physical quantities, like the differential cross section $\mathrm{d}\sigma^{Q\bar{Q}X}_{H_1H_2}$, have to be independent of both μ_R and μ_F. Finally, $\mathrm{d}\hat{\sigma}^{Q\bar{Q}X}_{ij}(p_1, p_2, \mu_R^2, \mu_F^2)$ describes the hard interaction of the partons i and j producing a heavy quark pair $Q\bar{Q}$. The interaction scale in this process is of the order of the heavy quark mass m. Since $m \gg \Lambda$, the strong coupling is small and the interaction is amenable to perturbation theory.

2.3 Leading and Next-to-leading order calculations

The hard scattering cross section $\mathrm{d}\hat{\sigma}^{Q\bar{Q}X}_{ij}$ may be calculated using a perturbative expansion in the strong coupling α_S. The differential cross section for heavy quark production in hadron-hadron collisions is then given by equation 2.7. A complete calculation of this differential cross section would be independent of the choice of the renormalization scale μ_R and the factorization scale μ_F. However, such full calculations are not possible and therefore the expansion is only calculated up to a finite order. In order to account for the dependence of the result on μ_R and μ_F, these scales are varied around a central

[1] DGLAP stands for Dokshitzer-Gribov-Lipatov-Altarelli-Parisi. These are the physicists who derived the evolution equation first.

value. The resulting variation in the differential cross section is then considered to be an uncertainty due to scale dependence.

The leading order contributions, that is terms with α_S^2, to the production cross section of heavy quarks are given by the processes

$$q\bar{q} \longrightarrow Q\bar{Q} \quad \text{and} \quad gg \longrightarrow Q\bar{Q} \; .$$

Some typical Feynman diagrams corresponding to these processes are illustrated in figure 2.3. For high partonic center of mass enegies, the contributions from $q\bar{q}$ vanish and

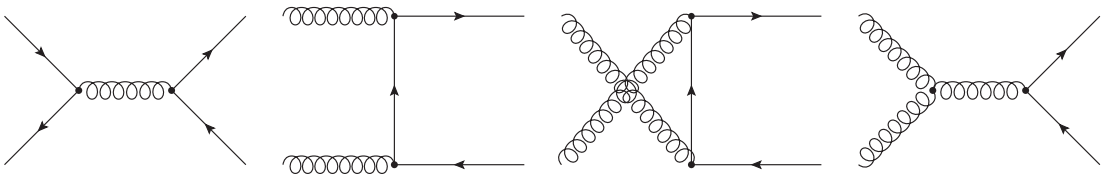

Figure 2.3: Leading order Feynman diagrams contributing to the cross section.

the remaining contributions from gg processes dominate. For the virtuality q^2 in the s-channel we have $\hat{s} \geq 4m^2$ and in the t-channel we have $\hat{t} \geq m^2$. Therefore, there are no poles in the propagators and the minimum transverse momentum transferred in the t-channel sets the scale for the renormalization. Since this is of the order of the heavy quark mass m and since m is much larger than Λ, the strong coupling α_S is small and perturbative calculations are possible.

Next-to-Leading order (NLO) calculations including terms of order α_S^3 are provided in [10] and [11] among others. From these calculations we expect that the uncertainties related to the renormalization scale μ_R and factorization scale μ_F should be reduced. However, these results still have a considerable dependence on the scales especially for large transverse momenta p_T of the heavy quark. Furthermore, large logarithms of the ratio p_T/m arise for $p_T \gg m$. They can be classified as leading logarithmic (LL) terms $\alpha_S^2(\alpha_S \log(p_T/m))^k$ and next-to-leading logarithmic (NLL) terms $\alpha_S^3(\alpha_S \log(p_T/m))^k$. These large logarithms are mainly caused by gluon-splitting and flavour-excitation diagrams, which are depicted in figure 2.4. Therefore, the NLO calculation only appropriately describes the heavy quark production for p_T of the order of the heavy quark mass m.

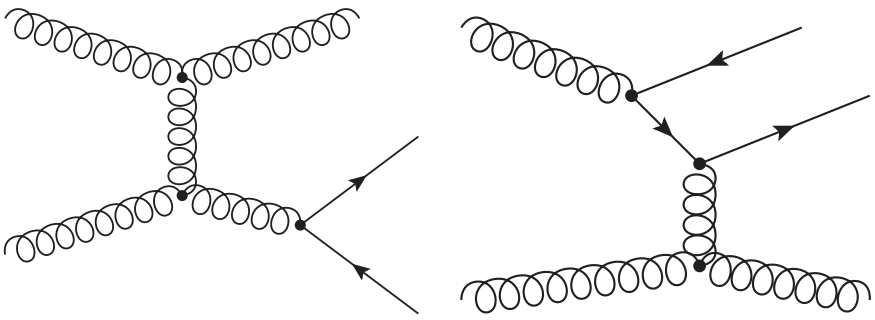

Figure 2.4: The left diagram illustrates the gluon-splitting and the right diagram depicts the flavour-excitation processes. Both are NLO contibutions causing large logarithms of the ratio p_{T}/m.

2.4 Resummation

The large logarithms arising in the NLO calculation for $p_{\mathrm{T}} \gg m$ can be resummed using the fragmentation function formalism. These calculations are described in detail in [12]. The idea of the formalism is depicted in figure 2.5. The heavy quark production differential cross section is then given by

$$\mathrm{d}\sigma_{H_1H_2}^{Q\bar{Q}X} = \sum_{i,j,k} \int \mathrm{d}x_1 \int \mathrm{d}x_2 \int \mathrm{d}x_3 \, F_{H_1}^i(x_1,\mu_F^2) F_{H_2}^j(x_2,\mu_F^2) \, \mathrm{d}\hat{\sigma}_{ij}^{kX}(p_1,p_2,\mu_R^2,\mu_F^2) D_k^Q(x_3,\mu_F^2) \, . \tag{2.8}$$

We can observe that this formula is very similar to the one given in equation 2.7. As there, $F_{H_1}^i(x_1,\mu_F^2)$ and $F_{H_2}^j(x_2,\mu_F^2)$ are the parton distribution functions of the colliding hadrons H_1 and H_2. The differences are as follows.

1. If a quark is produced at very high transverse momentum p_{T} with respect to the quark mass m (i.e. $p_{\mathrm{T}} \gg m$), then the mass has only a minor effect on the scattering process. Therefore, $\mathrm{d}\hat{\sigma}_{ij}^{kX}(p_1,p_2,\mu_R^2,\mu_F^2)$ describes the differential cross section for the production of a massless parton k with a four-momentum p_3 in the interaction of two parton i and j, originating from the colliding hadrons.

2. The heavy quark Q is produced trough the fragmentation of the massless parton k. The function $D_k^Q(x_3,\mu_F^2)$ is the perturbative fragmentation function. It describes the probability for a massless parton k to fragment into a heavy quark Q, which carries a (four-)momentum fraction x_3 of the parton k. The dependence on the factorization scale is determined by the DGLAP equations. A key property of this heavy quark

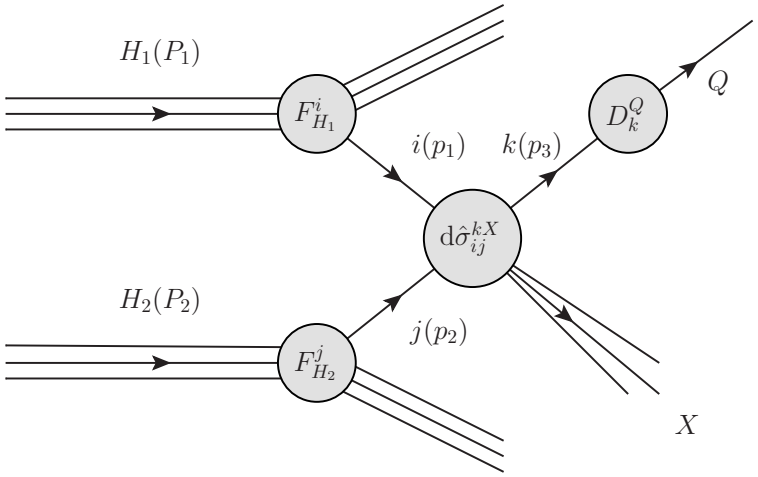

Figure 2.5: Diagram corresponding to the fragmentation function formalism. The diagram is very similar to figure 2.2. However here, k is a massless parton with four-momentum p_3 produced in the hard interaction of the partons i and j. The parton k fragments into a heavy quark Q. The fragmentaion is described by the fragmentation function D_k^Q.

fragmentation function is that its initial states conditions can be derived from first principles in QCD.

In this way, the large logarithms appearing in the NLO calculation are resummed through the scale dependence of the heavy quark fragmentation function $D_k^Q(x_3, \mu_F^2)$. This means, that they are accounted for in the very same way as the ultraviolet divergences are in the renormalization and the infrared and collinear divergences are in the factorization procedure. This kind of resummation has been performed to NLL accuracy and is provided in [12]. For $p_{\mathrm{T}} \gg m$ we have now a smaller dependence on the scales than in the NLO calculations. It is however difficult to recover the NLO results for p_{T} being of the order of m since for such transverse momenta the effects due to the heavy quark mass cannot be neglected. This has been resolved by combining NLO and the resummed results to describe the heavy quark production. In the next section we will introduce such an approach called Fixed-order next-to-leading logarithm (FONLL).

3 The FONLL Framework

Perturbative calculations to NLO accuracy describe the heavy quark production only for transverse momenta p_{T} of the heavy quark of the order of the heavy quark mass m and fail for $p_{\mathrm{T}} \gg m$ since then, large logarithms of the ratio p_{T}/m arise spoiling the convergence of the perturbative expansion. However, these large logarithms can be resummed to all orders using the fragmentation function approach as performed in [12] to NLL accuracy. This approach is appropriate for $p_{\mathrm{T}} \gg m$, but fails for p_{T} of the order of m since it is a massless formalism.

The acronym FONLL stands for fixed order plus next-to-leading logarithms and is a state-of-the-art calculation framework devised by M. Cacciari, M. Greco and P. Nason in [13]. In this framework, fixed order calculations to NLO accuracy are merged with NLL resummed results giving a suitable description of the heavy quark production. The differential cross section for heavy quark production in the FONLL framework is given by

$$\mathrm{d}\sigma_{\mathrm{FONLL}} = \mathrm{d}\sigma_{\mathrm{FO}} + G(m, p_{\mathrm{T}})(\mathrm{d}\sigma_{\mathrm{RS}} - \mathrm{d}\sigma_{\mathrm{FOM0}}) \,. \tag{3.1}$$

In this equation, $\mathrm{d}\sigma_{\mathrm{FO}}$ denotes the fixed next-to-leading order and $\mathrm{d}\sigma_{\mathrm{RS}}$ the resummed result. In order to merge the FO and RS calculations, terms already present in the FO calculations have to be subtracted from the RS result to avoid double counting. However, the RS calculations are given in the massless approximation. Therefore, the massless limit $\mathrm{d}\sigma_{\mathrm{FOM0}}$ of the FO result has to be taken into account. Then, one expects the difference $\mathrm{d}\sigma_{\mathrm{RS}} - \mathrm{d}\sigma_{\mathrm{FOM0}}$ being of the order α_{S}^4. In [13] though, it has been observed that this difference is in fact much larger than expected, especially for $p_{\mathrm{T}} \leq 5m$. For this reason, a function

$$G(m, p_{\mathrm{T}}) = \frac{p_{\mathrm{T}}^2}{p_{\mathrm{T}}^2 + k^2 m^2} \tag{3.2}$$

with $k = 5$ has been introduced to suppress the large difference for $p_{\mathrm{T}} \leq 5m$.

3.1 Fragmentation into hadrons

It is not possible to observe quarks as free particles since soon after their production, they are confined in color-neutral particles called hadrons. This is related to the scale dependence of the strong coupling α_{S} described in section 2.1. We observed there that

the interaction is strong for small energy scales or equivalently for large distances. For such scales, the strong coupling is large and perturbative calculations are not feasible. Therefore, the hadronization is described by non-perturbative fragmentation functions. The FONLL predictions for hadrons H_Q with a heavy quark Q are obtained through a convolution

$$\mathrm{d}\sigma^{H_Q}_{\mathrm{FONLL}} = \mathrm{d}\sigma^{Q}_{\mathrm{FONLL}} \otimes D_Q^{H_Q} \ , \tag{3.3}$$

where $\mathrm{d}\sigma^{Q}_{\mathrm{FONLL}}$ denotes the predicted differential cross section for the production of a heavy quark Q and $D_Q^{H_Q}$ is the non-perturbative fragmentation function. The function $D_Q^{H_Q}(z)$ describes the probability that a heavy quark Q hadronizes into a hadron H_Q, which has the four-momentum fraction z of the heavy quark.

The hadronization of bottom quarks b to hadrons H_b is parametrized by a Kartvelishvili et al. distribution

$$D_b^{H_b}(z) = (\alpha+1)(\alpha+2)z^{\alpha}(1-z) \tag{3.4}$$

in the context of FONLL calculations. The single parameter α of the distribution has been extracted from experimental data from LEP [14]. To account for uncertainties in the mass, α has been determined for three different values of the bottom mass. The values used for the mass of the bottom quark are $m_b = 4.50, 4.75, 5.00\,\mathrm{GeV}$ with the corresponding parameters $\alpha = 26.7, 24.2, 22.2$, where $m_b = 4.50\,\mathrm{GeV}$ with $\alpha = 24.2$ denotes the central value [15]. The functional form of the distribution is illustrated in figure 3.1.

The hadronization of charm quarks into D mesons D^0, D^+ and D^* is given by non-perturbative fragmentation functions which have been constructed in [16] using fragmentation functions describing the fragmentation of a heavy quark into a pseudoscalar and vector state provided in [17]. For the sake of brevity, we do not give the definitions of these functions here but note that these functions have a single free parameter r, which has been extracted from ALEPH e^+e^- data in [14]. Again, in order to account for uncertainties in the quark mass, the parameter r has been determined for three different values of the charm quark mass m_c. These values are $m_c = 1.3, 1.5, 1.7\,\mathrm{GeV}$ with the corresponding $r = 0.06, 0.1, 0.135$, where $m_c = 1.5\,\mathrm{GeV}$ with $r = 0.1$ denotes the central setting. The non-perturbative fragmentation functions for the charm hadronizing into a D meson are illustrated in figure 3.2.

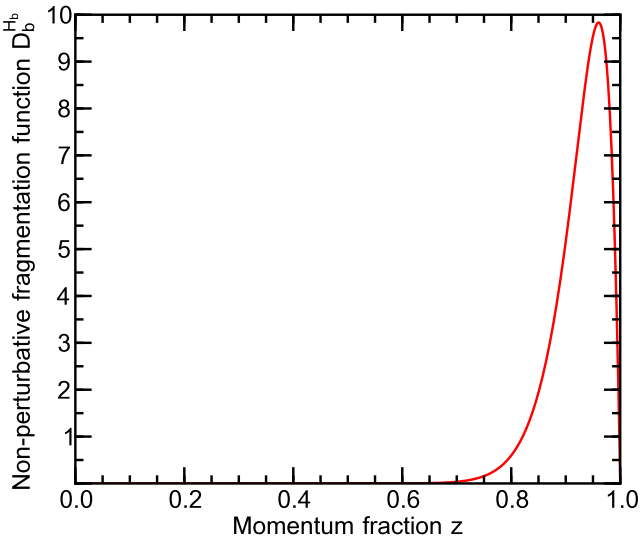

Figure 3.1: The Kartvelishvili et al. distribution with $\alpha = 24.2$. This distribution is used to describe the hadronization of a bottom quark b into a hadron H_b.

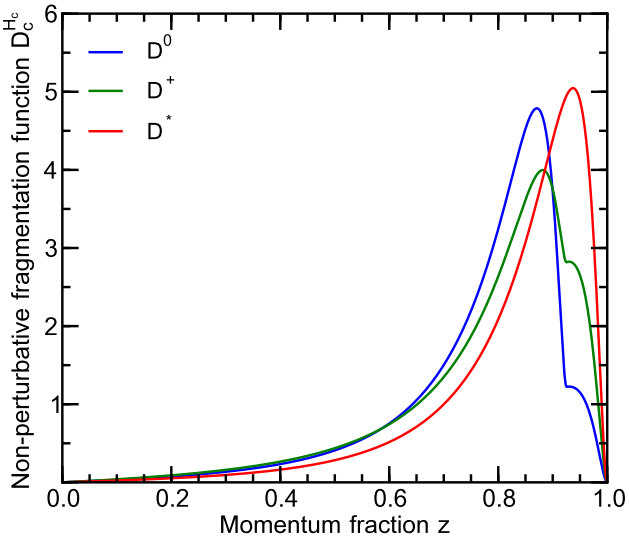

Figure 3.2: The non-perturbative fragmentation functions describing the hadronization of a charm quark c into one of the D mesons D^0, D^+ and D^* for the central parameter $r = 0.1$. The integrals are normalized to one.

In both cases we can observe, that the peak of the distributions is located near $z = 1$. This means that most of the hadrons H_Q will carry large momentum fractions z of the heavy quark Q. A qualitative explanation for this is, that the heavy quark Q is slowed down insignificantly when forming a hadron with lighter quarks. Therefore, the produced hadron H_Q has almost the whole four-momentum of the initial heavy quark Q. We can further observe, that the distributions describing the fragmentation of a charm quark into a D^0 and D^+ meson have two peaks, which represent the D^0 and D^+ mesons coming from the decay of D^* and D^0 and D^+ mesons originating directly from the hadronization of charm quarks.

3.2 Theoretical uncertainties

The FONLL calculations depend on the heavy quark mass m, the renormalization and factorization scales μ_R and μ_F and the parton distribution functions (PDF). An uncertainty is associated with each of these parameters. The determination of the uncertainties is described in the following.

To account for variations due to the scale dependence, the renormalization and factorization scales μ_R and μ_F are varied around the central value $\mu = (p_{\mathrm{T}}^2 + m^2)^{1/2}$ using the central values $m_b = 4.75\,\mathrm{GeV}$ for the mass of the bottom and $m_c = 1.5\,\mathrm{GeV}$ for the mass of the charm quark. Let $\xi_R = \mu_R/\mu$ and $\xi_F = \mu_F/\mu$. To avoid accidental compensations between both scale dependences of the calculated cross section, μ_R and μ_F are varied independently in the range $0.5 \leq \xi_R, \xi_F \leq 2.0$ with the constraint $0.5 \leq \xi_R/\xi_F \leq 2.0$. The cross section is calculated for the following settings of the renormalization and factorization scales relative to the central value μ:

$$(\xi_R, \xi_F) \in \{(1,1), (0.5,0.5), (2,2), (0.5,1), (1,0.5), (2,1), (1,2)\}\ .$$

The difference between the cross section corresponding to the central value $\xi_R = 1$, $\xi_F = 1$ and the envelope obtained by the variation is defined to be the uncertainty

$$\Delta(\mathrm{d}\sigma)_{\pm\mathrm{scale}}$$

related to the scale dependence of the differential cross section. The p_{T}-differential cross section of the charm quark for different scale settings is displayed in figure 3.3. In this figure, the ratio of the predictions for different scales over the central prediction is

depicted as well. We can observe that the scale variation is large for small p_{T} and is decreasing as p_{T} increases.

The values of the heavy quark mass used for the central calculations are $m_b = 4.75\,\mathrm{GeV}$ for bottom and $m_c = 1.5\,\mathrm{GeV}$ for charm quarks. To account for the dependence of the FONLL calculations on the heavy quark mass, the calculations are performed for three different values of the mass. These are $m_b = 4.50, 4.75, 5.00\,\mathrm{GeV}$ in the case of bottom and $m_c = 1.3, 1.5, 1.7\,\mathrm{GeV}$ for charm quarks. The parameters of the non-perturbative fragmentation functions are set to the corresponding values described in section 3.1. The renormalization and the factorization scale are set to $\mu = (p_{\mathrm{T}}^2 + m^2)^{1/2}$. Again, the envelope defines the uncertainty

$$\Delta(\mathrm{d}\sigma)_{\pm\mathrm{mass}}\ .$$

The variation of the charm quark p_{T}-spectrum due to mass variation is depicted in figure 3.4.

The last uncertainty accounted for is associated with the PDF set used for the calculation of the differential cross section. The default PDF set is CTEQ 6.6 [18]. The mass and the scales are set to their central values and the uncertainty related to the PDF set is evaluated as proposed in [19]. This defines again an uncertainty

$$\Delta(\mathrm{d}\sigma)_{\pm\mathrm{PDF}}\ .$$

Figure 3.5 illustrates the variation of the charm p_{T}-differential cross section due to the PDF uncertainty.

These three uncertainties combined in quadrature define the total uncertainty of the FONLL calculations. That is, the total uncertainty is given by

$$\Delta(\mathrm{d}\sigma)_{\pm} = \sqrt{\Delta(\mathrm{d}\sigma)^2_{\pm\mathrm{scale}} + \Delta(\mathrm{d}\sigma)^2_{\pm\mathrm{mass}} + \Delta(\mathrm{d}\sigma)^2_{\pm\mathrm{PDF}}}\ . \tag{3.5}$$

The FONLL calculation for the charm p_{T}-spectrum with the total uncertainty band is depicted in figure 3.6. If we compare this figure with the figures 3.3, 3.4 and 3.5, we observe, that the total uncertainty is by far dominated by the uncertainty due to scale variations.

FONLL predictions used within this thesis have been provided on the publicly accessible web page [20]. We used predictions for proton-proton collisions at $\sqrt{s} = 7\,\mathrm{TeV}$.

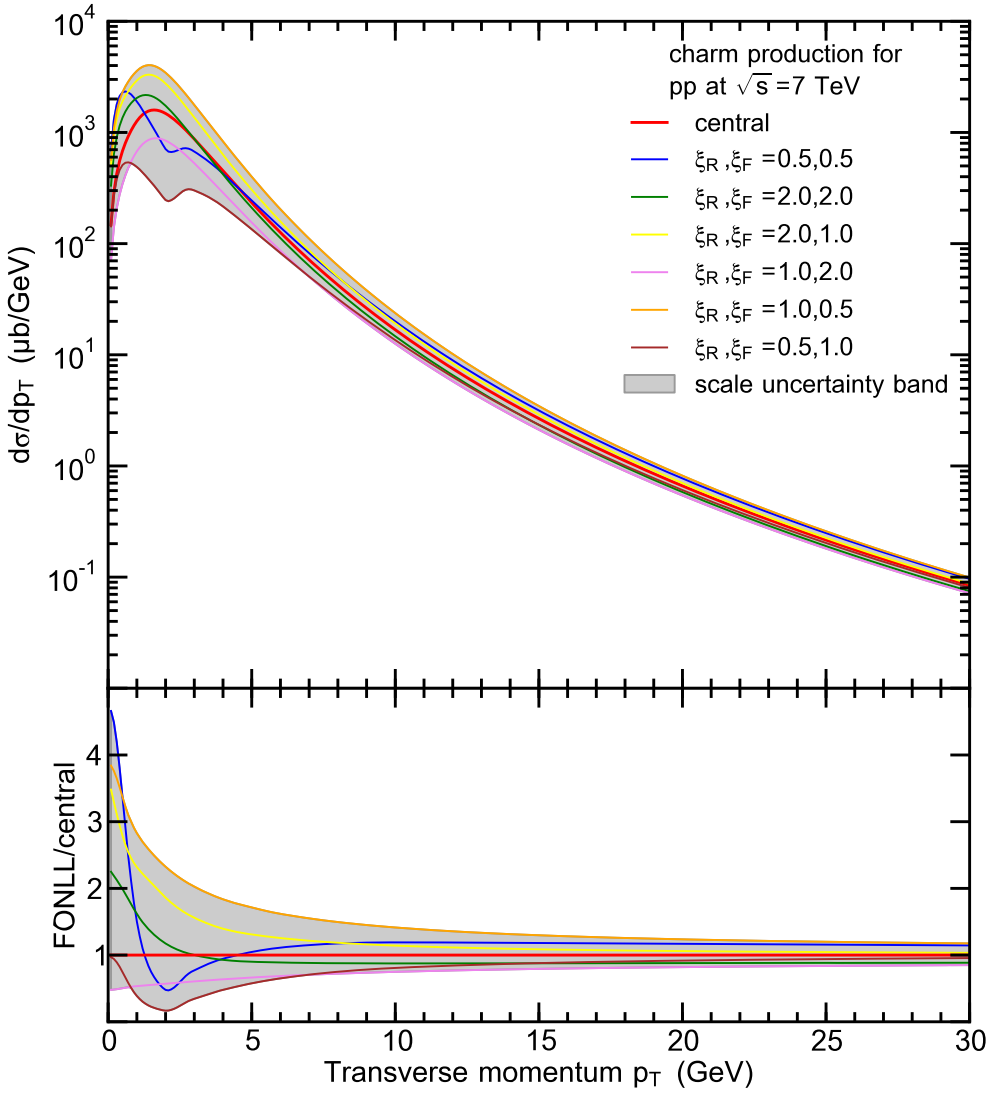

Figure 3.3: The p_{T}-differential cross section of the charm quark for different scales integrated over y. The grey shaded area defines the envelope of the scale variations and defines the uncertainty due to scale dependence.

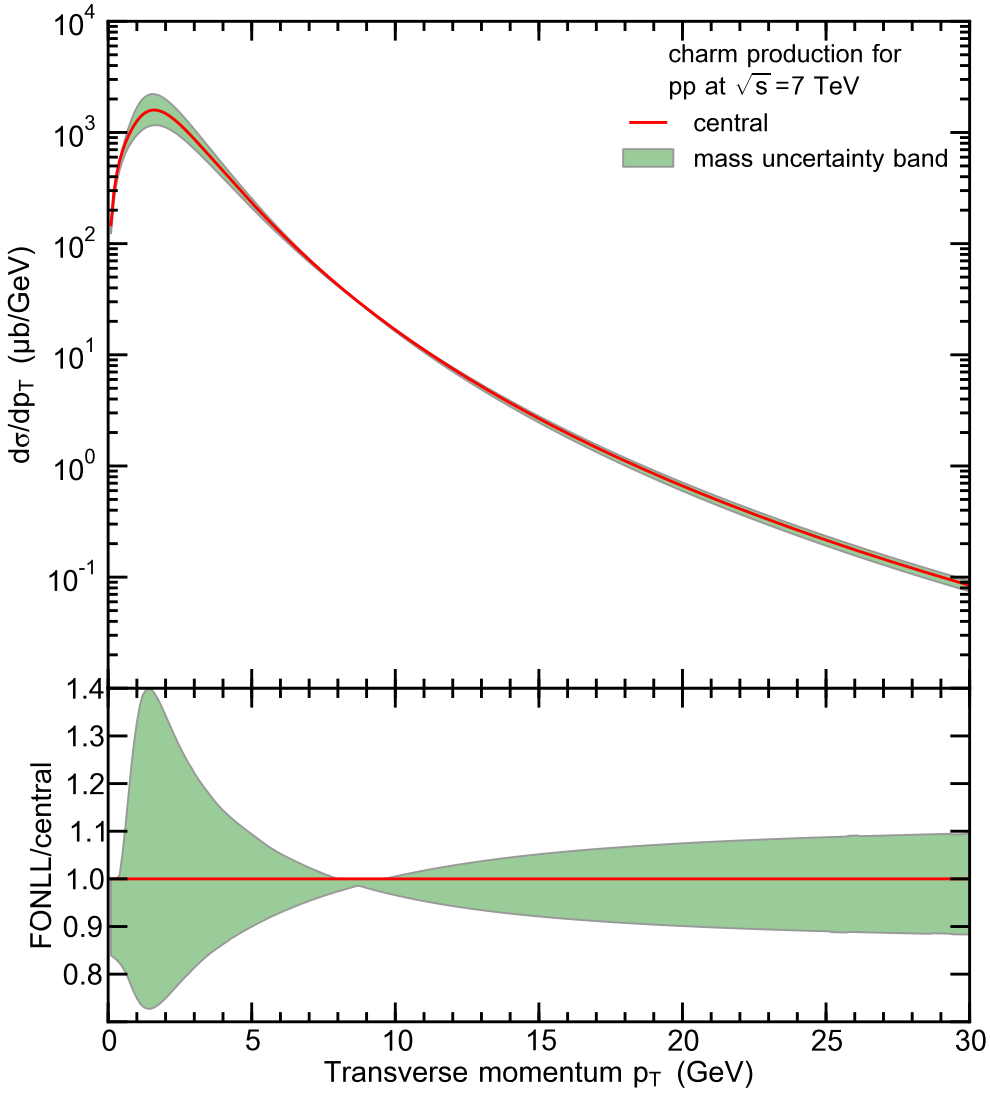

Figure 3.4: The p_{T}-spectrum of the charm quark for three different masses $m_c = 1.3, 1.5, 1.7\,\mathrm{GeV}$ integrated over all y. The variation of the charm mass to lower and higher values bounds the central cross section. The green area in between defines the uncertainty band of FONLL calculations due to variations of the charm mass.

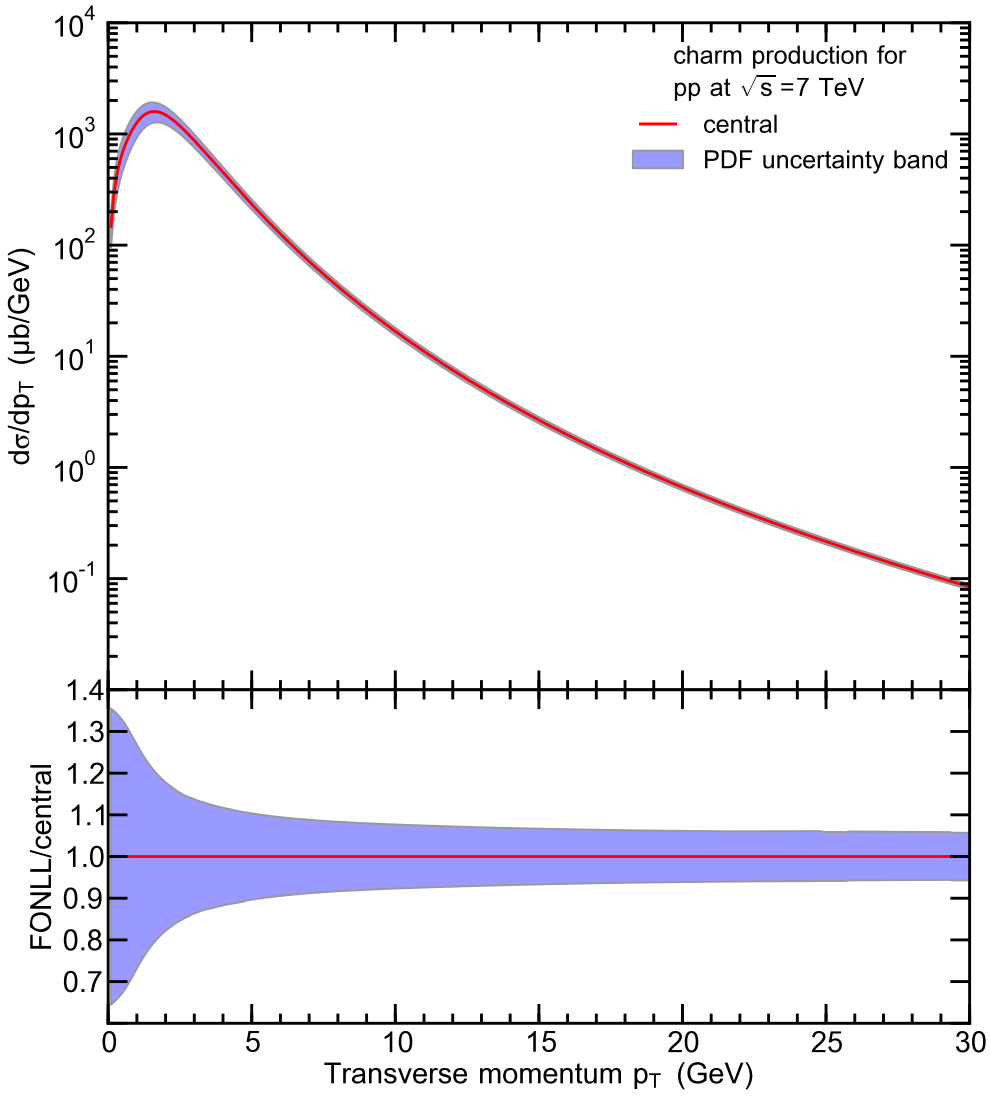

Figure 3.5: The variation of the charm p_{T}-spectrum integrated over all y due to the uncertainty related to the parton distribution function used for the calculation.

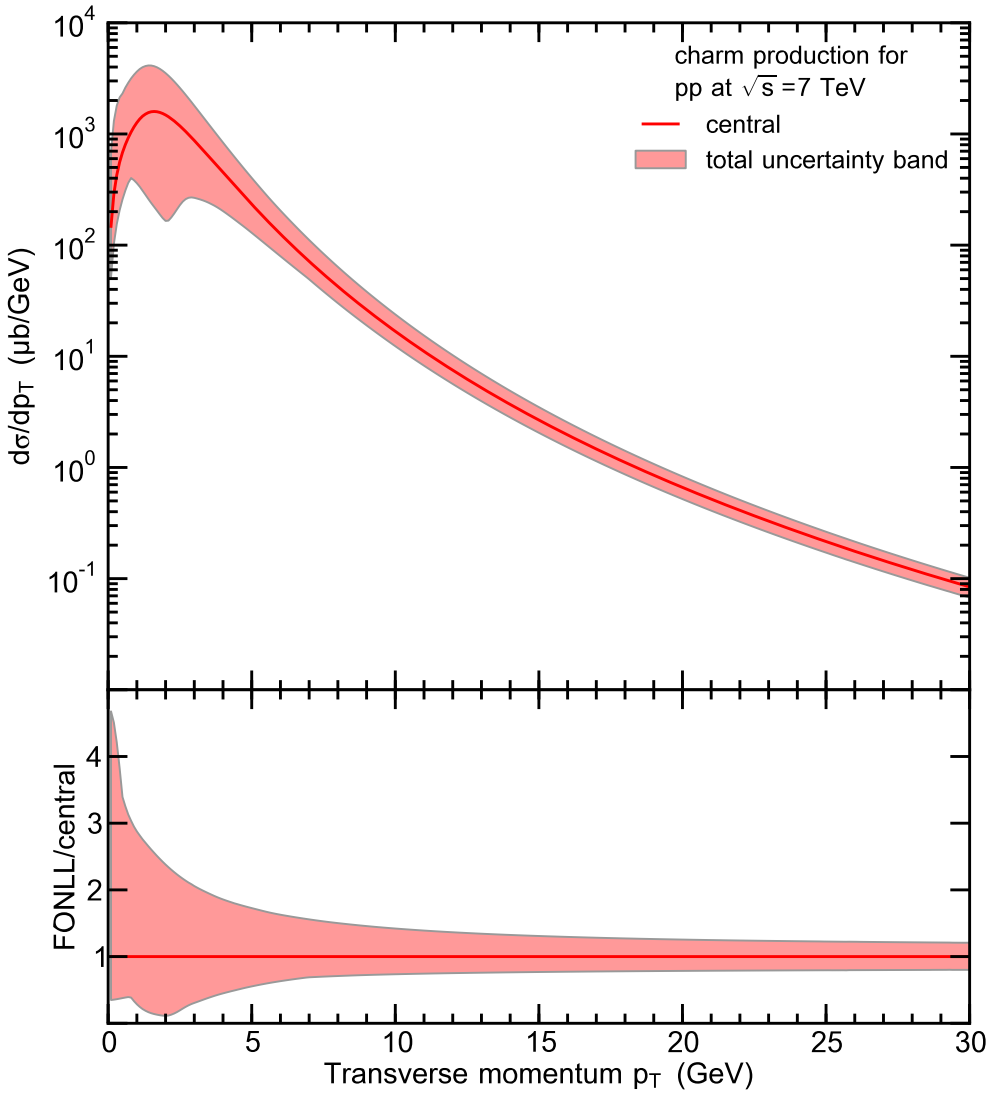

Figure 3.6: FONLL predictions for charm production in proton-proton collisions at $\sqrt{s} = 7\,\text{TeV}$. The p_T-spectrum with the total uncertainty band due to variations of the charm mass, the renormalization and factorization scales and due to uncertainties related to the parton distribution function is depicted.

Predictions have been provided for distribution in p_{T}, in y etc. as well as for the total cross section within p_{T} and y ranges specified by the user. It is also possible to make a choice between different PDF sets and fragmentation functions, but we used the default settings for our calculations. Results are provided for different settings of the parameters summarized as follows.

- `central` is the result corresponding to the central settings of the parameters. These are $m_b = 4.75\,\mathrm{GeV}$ for the bottom and $m_c = 1.5\,\mathrm{GeV}$ for the charm mass, $\xi_F = \xi_R = 1$ for the ratio of the factorization and renormalization scales relative to $\mu = (p_{\mathrm{T}}^2 + m^2)^{1/2}$.
- `min` is the lower boundary given by the difference of the central value and the uncertainty $\Delta(\mathrm{d}\sigma)_-$ as defined in equation 3.5.
- `max` is the upper boundary given by the sum of the central value and the uncertainty $\Delta(\mathrm{d}\sigma)_+$ as defined in equation 3.5.
- `min_sc` is the minimum of the cross sections obtained by the variation of the scales, that is

  $$\min\{\mathrm{d}\sigma_{(\xi_F,\xi_R)} \mid (\xi_F,\xi_R) \in \{(0.5,0.5),(2,2),(2,1),(1,2),(1,0.5),(0.5,1)\}\}$$

  for all p_{T} in the considered range.
- `max_sc` is the maximum of the cross sections obtained by the variation of the scales, that is

  $$\max\{\mathrm{d}\sigma_{(\xi_F,\xi_R)} \mid (\xi_F,\xi_R) \in \{(0.5,0.5),(2,2),(2,1),(1,2),(1,0.5),(0.5,1)\}\}$$

  for all p_{T} in the considered range.
- `min_mass` denotes the lower boundary of results obtained by varying the charm mass.
- `max_mass` denotes the upper boundary of results obtained by varying the charm mass.
- `min_pdf` denotes the lower boundary of results obtained by accounting for uncertainties related to the PDF.
- `max_pdf` denotes the upper boundary of results obtained by accounting for uncertainties related to the PDF.

- `fr=.5 .5` denotes the prediction obtained for setting the scales to $\xi_F = 0.5$ and $\xi_R = 0.5$.
- `fr= 2 2` denotes the prediction obtained for setting the scales to $\xi_F = 2.0$ and $\xi_R = 2.0$.
- `fr= 2 1` denotes the prediction obtained for setting the scales to $\xi_F = 2.0$ and $\xi_R = 1.0$.
- `fr= 1 2` denotes the prediction obtained for setting the scales to $\xi_F = 1.0$ and $\xi_R = 2.0$.
- `fr= 1 .5` denotes the prediction obtained for setting the scales to $\xi_F = 1.0$ and $\xi_R = 0.5$.
- `fr= .5 1` denotes the prediction obtained for setting the scales to $\xi_F = 0.5$ and $\xi_R = 1.0$.

4 Extrapolation

The general idea of the extrapolation is as follows. Suppose we have measured the integrated cross section of a certain particle X over a domain $A \subseteq \mathbb{R}_{\geq 0} \times \mathbb{R}$ of the (p_{T}, y) phase space, which we will call $\sigma_A^{\mathrm{expr}}(X)$. Further suppose, that there is a theoretical prediction for the double differential cross section $\frac{\mathrm{d}^2\sigma(X)}{\mathrm{d}(p_{\mathrm{T}}^2)\mathrm{d}y}$ of the considered particle X for the whole phase space. Our aim is to extrapolate the integrated cross section for a domain B of the phase space using the measured and predicted cross sections. To this aim we calculate

$$\sigma_A^{\mathrm{theo}}(X) = \int_A \frac{\mathrm{d}^2\sigma(X)}{\mathrm{d}(p_{\mathrm{T}}^2)\mathrm{d}y}\, \mathrm{d}(p_{\mathrm{T}}^2)\, \mathrm{d}y\ , \tag{4.1}$$

$$\sigma_B^{\mathrm{theo}}(X) = \int_B \frac{\mathrm{d}^2\sigma(X)}{\mathrm{d}(p_{\mathrm{T}}^2)\mathrm{d}y}\, \mathrm{d}(p_{\mathrm{T}}^2)\, \mathrm{d}y\ . \tag{4.2}$$

$\sigma_A^{\mathrm{theo}}(X)$ is the predicted integrated cross section for the measured region A and $\sigma_B^{\mathrm{theo}}(X)$ is the predicted integrated cross section for the domain B of the extrapolation. To obtain the extrapolated cross section $\sigma_B^{\mathrm{extr}}(X)$ for the domain B, we simply assume

$$\sigma_B^{\mathrm{extr}}(X)/\sigma_B^{\mathrm{theo}}(X) = \sigma_A^{\mathrm{expr}}(X)/\sigma_A^{\mathrm{theo}}(X)\ . \tag{4.3}$$

The notion of this assumption is that the ratio of the number of particles X we expect to observe in the domain B of the phase space to the predicted number of particles for the same domain is equal to the ratio of the number of particles we already measured in the domain A to the number of particles predicted by the theory for the domain A of the measurement. So essentially, we assume that the theoretical predictions we are using describe at least the shape of the cross section of the considered particle X appropriately such that the ratio of the measured and predicted cross sections are constant. Equation 4.3 defines the extrapolated cross section. We can write this equation in the more convenient form

$$\sigma_B^{\mathrm{extr}}(X) = \sigma_A^{\mathrm{expr}} \cdot f_A^B(X)\ , \tag{4.4}$$

where we introduced the extrapolation factor $f_A^B(X) = \sigma_B^{\mathrm{theo}}(X)/\sigma_A^{\mathrm{theo}}(X)$.

In the course of this section, we will describe the single ingredients of the extrapolation procedure. We will start by explaining the general methods used by the ALICE and LHCb collaborations to measure charm production in proton-proton collisions at $\sqrt{s} =$

7 TeV and present the integrated cross sections of charmed hadrons measured by these two collaborations. Then, we will explain how these measured cross sections have been combined to use them for the extrapolation of the different charmed hadrons followed by the description of theoretical predictions used to describe the cross sections of the measured particles. Finally, we will explain how cross sections have been extrapolated and how uncertainties have been propagated.

4.1 Measurement of charm production

Due to confinement, charm quarks produced in proton-proton collisions cannot be observed as free particles since they hadronize soon after their production. The probability for a charm quark to form a charmed hadron of a certain kind is called fragmentation fraction. These have been measured in e^+e^- annihilation processes by several groups [21]. The ratios are depicted in figure 4.1. Although it is not possible to measure charm

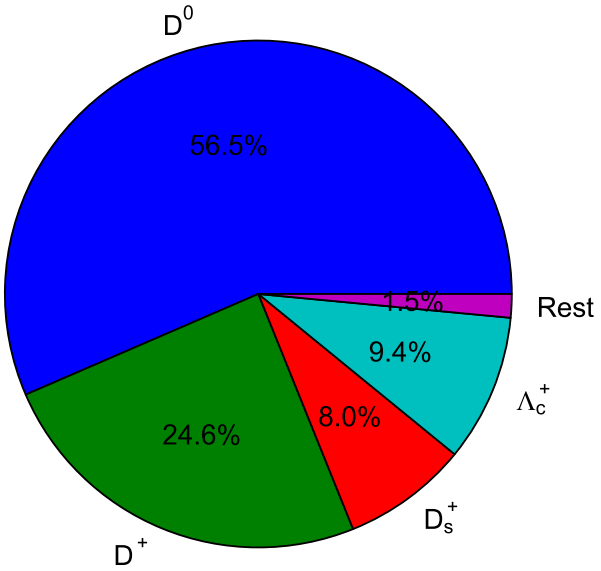

Figure 4.1: The fragmentation fractions for a charm quark hadronizing into a charmed hadron. The values for the fractions have been taken from [21].

production directly, the production of charmed hadrons can be measured principally.

Using then the fragmentation fractions, one can obtain the charm production cross section from these measurements. Furthermore, if we measure cross sections of D^0, D^+, D_s^+ and Λ_c^+ originating from the hadronization of charm quarks, we can obtain the charm pair cross section by adding up the single conrtibutions assuming that the residual 1% is negligible. In measurements of charmed hadron production, it has to be taken into account that there are two sources. The first source is the hadronization of charm quarks produced in proton-proton collisions for instance. These charmed hadrons will be called prompt hadrons. The second source is the decay of bottomed hadrons. Since hadrons from these decays do not originate from charm quarks produced in the collision, this source is considered to be background. Another challange is that charmed hadrons have short lifetimes. Their decay length is of the order of few 100 μm and therefore they decay before they can be observed. However, it is possible to reconstruct these hadrons from their decay products using invariant mass reconstruction.

Suppose a particle X with four-momentum p_X decays into the particles $A_1, A_2, \ldots, A_N$ with four-momenta $p_1, p_2, \ldots, p_N$. The reaction is given by

$$X \longrightarrow A_1 + A_2 + \cdots + A_N \; . \tag{4.5}$$

Since energy and momentum are conserved, it holds

$$p_X = \sum_{i=1}^{N} p_i \; . \tag{4.6}$$

Taking the square of both sides of this equation we obtain

$$m_X^2 = p_X^2 = \left(\sum_{i=1}^{N} p_i \right)^2 = \left(\sum_{i=1}^{N} E_i \right)^2 - \left(\sum_{i=1}^{N} \vec{p}_i \right)^2 \; . \tag{4.7}$$

This means that, if we can measure the energies E_i and the momenta $\vec{p}_i$ of the decay products, we can reconstruct the mass of the decayed particle and identify it. However, since not all particles $A_1, A_2, \ldots, A_N$ detected orginate from the decay process, there will be a so-called combinatorial background due to combinations of uncorrelated particles. Combinations of particles originating from the decay of the particle X will then cause a peak in the invariant mass spectrum at the mass m_X of the decayed particle X. Unfortunately, the combinatorial background can become rather large especially for decay processes with many decay products and can conceal the peak in the invariant mass spectrum. Thus, a preselection of the detected particles is performed using a

lifetime tag. That is, only such detected particles are considered for the invariant mass analysis, which originate from a common displaced vertex with respect to the primary interaction vertex. The displacement is required to be of the order of the decay length of particle X. This preselection reduces the combinatorial background and improves the signal to background ratio. As an example, the invariant mass spectrum for the decay channel $D^+ \to K^-\pi^+\pi^+$ measured by ALICE for different ranges of the transverse momentum p_T from [4] is given in figure 4.2. We can observe a peak at approximately 1.87 GeV, which corresponds to the mass $m = 1869.69 \pm 0.16\,\mathrm{MeV}$ [8] of the D^+ meson. The width of the Gaussian peak is determined by the experimental resolution.

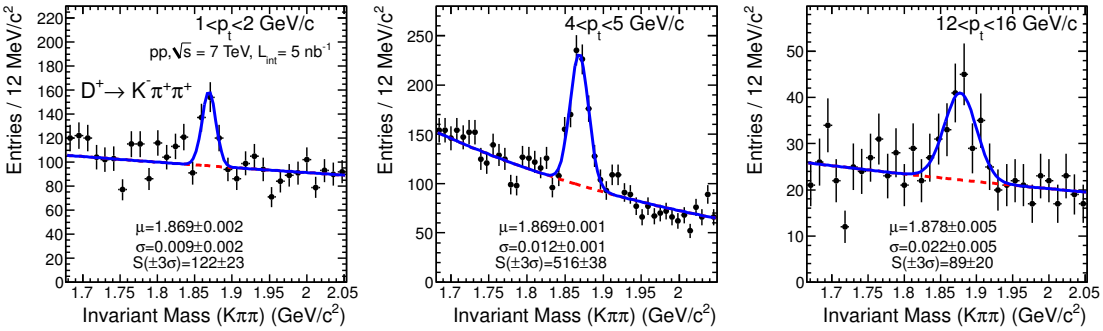

Figure 4.2: Invariant mass spectrum for the decay $D^+ \to K^-\pi^+\pi^+$ measured in [4]. You can observe the peaks at approximately 1.87 GeV, which corresponds to the mass $m = 1869.69 \pm 0.16\,\mathrm{MeV}$ [8] of the D^+ meson.

Usually, the number of decays $X \to A_1 + A_2 + \cdots + A_N$ is measured for several bins in p_T and y. The integrated cross section of the particle X over a bin i is then given by

$$\sigma_i(X) = \frac{N_i(X \to A_1 + \cdots + A_N)}{\varepsilon_i(X \to A_1 + \cdots + A_N) \cdot \mathcal{B}(X \to A_1 + \cdots + A_N) \cdot \mathcal{L}_\mathrm{int}} \,. \tag{4.8}$$

In this equation, $N_i(X \to A_1 + \cdots + A_N)$ is the number of decays measured in bin i for the considered decay channel $X \to A_1 + \cdots + A_N$, $\mathcal{B}(X \to A_1 + \cdots + A_N)$ is the branching ratio of the decay channel, $\varepsilon_i(X \to A_1 + \cdots + A_N)$ denotes the efficiency of the detector for the bin i and for the channel observed and $\mathcal{L}_\mathrm{int}$ is the integrated luminosity. The respective differential cross sections can be obtained by dividing this result with the binwidth in p_T or with the binwidth in y.

ALICE measured charm production at central rapidity $|y| < 0.5$ in proton-proton collisions at $\sqrt{s} = 7\,\mathrm{TeV}$ [4], [5]. The p_T-differential cross section of the prompt charmed

mesons D^0, D^+, D^{*+} and D_s^+ in $|y| < 0.5$ were measured. The measurements have been performed with an integrated luminosity of $\mathcal{L}_{\text{int}} = 5\,\text{nb}^{-1}$ for the measurement of D^0, D^+ and D^{*+} and with $\mathcal{L}_{\text{int}} = 4.98\,\text{nb}^{-1}$ for the measurement of D_s^+. The relative uncertainty of the integrated luminosity was 3.5% in both cases. LHCb measured also p_{T}-differential cross section but of D^0, D^+, D^{*+}, D_s^+ and Λ_c^+ in proton-proton collisions at $\sqrt{s} = 7\,\text{TeV}$ for $2.0 < y < 4.5$. These measurements have been performed with an integrated luminosity of $\mathcal{L}_{\text{int}} = 15\,\text{nb}^{-1}$ which has a relative uncertainty of 3.5% as well. The decay channels used to reconstruct the charmed hadrons from their decay products as described above are given in table 4.1. Note, that the cross sections given for D^0

Decay channel	Branching ratio
$D^0 \to K^-\pi^+$	$(3.88 \pm 0.05)\%$
$D^+ \to K^-\pi^+\pi^+$	$(9.13 \pm 0.19)\%$
$D^{*+} \to D^0\pi^+$	$(67.7 \pm 0.5)\%$
$D_s^+ \to \phi\pi^+ \to K^-K^+\pi^+$	$(2.28 \pm 0.12)\%$
$\Lambda_c^+ \to pK^-\pi^+$	$(5.0 \pm 1.3)\%$

Table 4.1: The decay channels used by ALICE and LHCb to reconstruct the charmed hadron yields. The branching ratios have been taken from [8].

and D^+ already include feeddown from D^{*+}. Although both experiments measured charm production in proton-proton collisions at $\sqrt{s} = 7\,\text{TeV}$, the phase space covered is different. The domain measured by ALICE for the different D mesons are given as follows

$$A_{D^0}^{\text{ALICE}} = \{(p_{\text{T}}, y) \in (1, 16) \times (-0.5, 0.5) \mid p_{\text{T}} \text{ in GeV}\} \tag{4.9}$$

$$A_{D^+}^{\text{ALICE}} = \{(p_{\text{T}}, y) \in (1, 24) \times (-0.5, 0.5) \mid p_{\text{T}} \text{ in GeV}\} \tag{4.10}$$

$$A_{D^{*+}}^{\text{ALICE}} = \{(p_{\text{T}}, y) \in (1, 24) \times (-0.5, 0.5) \mid p_{\text{T}} \text{ in GeV}\} \tag{4.11}$$

$$A_{D_s^+}^{\text{ALICE}} = \{(p_{\text{T}}, y) \in (2, 12) \times (-0.5, 0.5) \mid p_{\text{T}} \text{ in GeV}\} \tag{4.12}$$

The integrated cross sections for the measured D mesons over their respective integration domains are provided in [22] and [5]. In [22] however, only the statistical and systematic

uncertainties are cited. If $\sigma(X)$ denotes the cross section summed over all bins, that is

$$\sigma(X) = \sum_i \sigma_i(X) \,, \tag{4.13}$$

where $\sigma_i(X)$ denotes the integrated cross section in bin i as given in equation 4.8, then the uncertainties resulting from the uncertainty of the integrated luminosity and resulting from the uncertainty of the branching ratios can be obtained using Gaussian propagation of uncertainty. So, these uncertainties are given by

$$(\Delta\sigma(X))_{\pm\text{lum}} = \sigma(X) \cdot \Delta\mathcal{L}_{\text{int}}/\mathcal{L}_{\text{int}} \,, \tag{4.14}$$

$$(\Delta\sigma(X))_{\pm\text{BR}} = \sigma(X) \cdot \Delta\mathcal{B}/\mathcal{B} \,. \tag{4.15}$$

The integrated cross sections measured by ALICE are summarized in table 4.2.

Hadron	σ_{ALICE}	stat.	syst.	lum.	BR
D^0	412.2	± 32.7	$^{+55.2}_{-139.5}$	± 14.4	± 5.3
D^+	198.3	± 24.0	$^{+41.8}_{-73.2}$	± 6.9	± 4.1
D^{*+}	203.3	± 22.7	$^{+30.0}_{-67.0}$	± 7.1	± 3.0
D_s^+	53.0	± 12.0	$^{+13.0}_{-15.0}$	± 2.0	± 3.0

Table 4.2: The integrated cross sections in units of μb of the D mesons over the respective ranges given in the equations 4.9 to 4.12 measured by ALICE. The values with the statistical and systematic uncertainties have been taken from [22] and [5]. The uncertainties due to uncertainties of the integrated luminosity (lum.) and due to uncertainties of the branching ratios (BR) have been calculated using equations 4.14 and 4.15.

LHCb measured the production within $0 < p_{\text{T}} < 8\,\text{GeV}$ and $2.0 < y < 4.5$ in bins of the width 1 GeV in p_{T} and 0.5 in y except for Λ_c^+. For Λ_c^+, bin-integrated cross sections have been provided for bins of the width 0.5 in the rapidity range $2.0 < y < 4.0$ integrated over $2\,\text{GeV} < p_{\text{T}} < 8\,\text{GeV}$ and for bins of the width 1 GeV within $2\,\text{GeV} < p_{\text{T}} < 8\,\text{GeV}$ integrated over $2.0 < y < 4.5$. We will use the latter measurement, since it covers a larger rapidity range. Only such bins have been used for the analysis in [6] where the relative uncertainty of the cross section in that bin was smaller than 50%. Cross sections for the

empty bins have been extrapolated using the remaining bins and prediction obtained from the event generator PYTHIA 6. Therefore, the integrated cross sections of prompt charmed hadrons cited in [6] are extrapolated results. In this work however, we will only use such bins where measured cross sections are provided. The integration domains for the different charmed hadrons measured by LHCb are then given by

$$\begin{aligned} A_{D^0}^{\mathrm{LHCb}} = &\{(p_{\mathrm{T}}, y) \in (0,8) \times (2.0, 2.5) \cup (0,8) \times (2.5, 3.0) \cup (0,8) \times (3.0, 3.5) \cup \\ &(0,8) \times (3.5, 4.0) \cup (0,6) \times (4.0, 4.5) \mid p_{\mathrm{T}} \text{ in GeV}\} \ , \end{aligned} \tag{4.16}$$

$$\begin{aligned} A_{D^+}^{\mathrm{LHCb}} = &\{(p_{\mathrm{T}}, y) \in (1,8) \times (2.0, 2.5) \cup (0,8) \times (2.5, 3.0) \cup (0,8) \times (3.0, 3.5) \cup \\ &(0,8) \times (3.5, 4.0) \cup (0,6) \times (4.0, 4.5) \mid p_{\mathrm{T}} \text{ in GeV}\} \ , \end{aligned} \tag{4.17}$$

$$\begin{aligned} A_{D^{*+}}^{\mathrm{LHCb}} = &\{(p_{\mathrm{T}}, y) \in (3,8) \times (2.0, 2.5) \cup (1,8) \times (2.5, 3.0) \cup (0,7) \times (3.0, 3.5) \cup \\ &(0,7) \times (3.5, 4.0) \cup (0,5) \times (4.0, 4.5) \mid p_{\mathrm{T}} \text{ in GeV}\} \ , \end{aligned} \tag{4.18}$$

$$\begin{aligned} A_{D_s^+}^{\mathrm{LHCb}} = &\{(p_{\mathrm{T}}, y) \in (1,8) \times (2.0, 2.5) \cup (1,7) \times (2.5, 3.0) \cup (0,8) \times (3.0, 3.5) \cup \\ &(1,6) \times (3.5, 4.0) \cup (2,4) \times (4.0, 4.5) \mid p_{\mathrm{T}} \text{ in GeV}\} \ , \end{aligned} \tag{4.19}$$

$$A_{\Lambda_c^+}^{\mathrm{LHCb}} = \{(p_{\mathrm{T}}, y) \in (2,8) \times (2.0, 4.5) \mid p_{\mathrm{T}} \text{ in GeV}\} \ . \tag{4.20}$$

The corresponding integrated cross section have been obtained from internal analysis notes [23]. There, it was distinguished between systematics and global systematics. The global systematics is the quadratic sum of the uncertainty of the track efficiency and of the luminosity. However, to be consitent with the uncertainties cited by ALICE, these uncertainties have been rearanged. The uncertainties due to uncertainties of the track efficiency have been added quadratically to the systematic uncertainties cited in the analysis note giving a new systematic uncertainty. The results as we will use them in this work are summarized in table 4.3.

4.2 Combination of ALICE and LHCb measurements

ALICE measured charm production in proton-proton collisions at $\sqrt{s} = 7\,\mathrm{TeV}$ for the central rapidity range $|y| < 0.5$ and LHCb measured for the forward rapidity interval $2.0 < y < 4.5$. Since the charm production is symmetric with respect to the rapidity y, a measurement of the cross section in some domain $A \subseteq \mathbb{R}_{\geq 0} \times \mathbb{R}$ of the (p_{T}, y) phase space defines also the cross section in the region $\bar{A} = \{(p_{\mathrm{T}}, y) \in \mathbb{R}_{\geq 0} \times \mathbb{R} \mid (p_{\mathrm{T}}, -y) \in A\}$. Therefore, when combining the integrated cross sections from ALICE and LHCb

Hadron	σ_{LHCb}	stat.	syst.	lum.	BR
D^0	827.9	± 8.0	± 55.7	± 29.0	± 10.8
D^+	302.9	± 5.0	± 31.7	± 10.6	± 6.4
D^{*+}	252.5	± 9.7	± 27.1	± 8.9	± 3.8
D_s^+	74.1	± 5.4	± 8.6	± 2.6	± 4.3
Λ_c^+	88.9	± 9.9	± 13.9	± 3.1	± 23.1

Table 4.3: The integrated cross sections in units of μb of the charmed hadrons measured by LHCb in proton-proton collisions at $\sqrt{s} = 7\,\mathrm{TeV}$. The integration domains are given in the equations 4.16 to 4.20.

measurements, we can account for this symmetry by double-weighting the results of LHCb. The combined integration domains of the different charmed hadrons are then

$$A_1 = A_{D^0}^{\mathrm{ALICE}} \cup A_{D^0}^{\mathrm{LHCb}} \cup \bar{A}_{D^0}^{\mathrm{LHCb}} \,, \tag{4.21}$$

$$A_2 = A_{D^+}^{\mathrm{ALICE}} \cup A_{D^+}^{\mathrm{LHCb}} \cup \bar{A}_{D^+}^{\mathrm{LHCb}} \,, \tag{4.22}$$

$$A_3 = A_{D^{*+}}^{\mathrm{ALICE}} \cup A_{D^{*+}}^{\mathrm{LHCb}} \cup \bar{A}_{D^{*+}}^{\mathrm{LHCb}} \,, \tag{4.23}$$

$$A_4 = A_{D_s^+}^{\mathrm{ALICE}} \cup A_{D_s^+}^{\mathrm{LHCb}} \cup \bar{A}_{D_s^+}^{\mathrm{LHCb}} \,, \tag{4.24}$$

$$A_5 = A_{\Lambda_c^+}^{\mathrm{LHCb}} \cup \bar{A}_{\Lambda_c^+}^{\mathrm{LHCb}} \,. \tag{4.25}$$

The combined cross sections have then be calculated accordingly and are given by the equations

$$\sigma_{A_1}^{\mathrm{expr}}(D^0) = \sigma_{\mathrm{ALICE}}(D^0) + 2 \cdot \sigma_{\mathrm{LHCb}}(D^0) \,, \tag{4.26}$$

$$\sigma_{A_2}^{\mathrm{expr}}(D^+) = \sigma_{\mathrm{ALICE}}(D^+) + 2 \cdot \sigma_{\mathrm{LHCb}}(D^+) \,, \tag{4.27}$$

$$\sigma_{A_3}^{\mathrm{expr}}(D^{*+}) = \sigma_{\mathrm{ALICE}}(D^{*+}) + 2 \cdot \sigma_{\mathrm{LHCb}}(D^{*+}) \,, \tag{4.28}$$

$$\sigma_{A_4}^{\mathrm{expr}}(D_s^+) = \sigma_{\mathrm{ALICE}}(D_s^+) + 2 \cdot \sigma_{\mathrm{LHCb}}(D_s^+) \,, \tag{4.29}$$

$$\sigma_{A_5}^{\mathrm{expr}}(\Lambda_c^+) = 2 \cdot \sigma_{\mathrm{LHCb}}(\Lambda_c^+) \,, \tag{4.30}$$

where σ_{ALICE} and σ_{LHCb} denote the cross sections measured by ALICE and LHCb and they are given in the tables 4.2 and 4.3. The statistical uncertainties have been propagated using Gaussian propagation of uncertainties. For the combination of the asymmetric

systematic uncertainties, it is argued for example in [24] that the combination of the uncertainties using Gaussian propagation law separately is not always appropriate. There, two models for the addition of asymmetric uncertainties have been introduced and a web application is provided to calculate the combined uncertainty for each model. However, we observed, that the difference between the combination of the uncertainties separately and the combination of them using one of the models described in that paper is not significant. Therefore, we propagate the contributions of the asymmetric systematic uncertainty separately using Gaussian propagation. The measurement of the luminosity for each experiment has been performed separately but the determination of the beam intensity part of this measurement is linearly correlated between the experiments. However, we do not know the contributions of the respective parts and therefore we assume the uncertainty to be uncorrelated and combine them using Gaussian propagation of uncertainties. The branching ratios used by both experiments have been provided by [8]. Therefore, they are 100% correlated and the uncertainties due to the branching ratios have been added linearly. The results for the combined cross sections are given in table 4.4.

Hadron	σ	stat.	syst.	lum.	BR
D^0	2067.9	± 36.4	$^{+124.2}_{-178.5}$	± 59.7	± 26.8
D^+	804.0	± 26.0	$^{+75.9}_{-96.8}$	± 22.3	± 16.8
D^{*+}	708.2	± 29.8	$^{+61.8}_{-86.1}$	± 19.1	± 10.6
D_s^+	201.1	± 16.1	$^{+21.6}_{-22.8}$	± 5.6	± 11.6
Λ_c^+	177.7	± 19.8	$^{+27.7}_{-27.7}$	± 6.2	± 46.2

Table 4.4: The combination of the integrated cross sections measured by ALICE and LHCb in units of μb. The covered domains of the phase space are given by the equations 4.21 to 4.25. Note that the results from LHCb have been multiplied with two since the charm distribution is symmetric with respect to the rapidity y.

4.3 Theoretical predictions and comparison

Theoretical predictions for the charmed mesons D^0, D^+ and D^{*+} have been calculated using the FONLL framework. The calculations include theoretical uncertainties due to variations of the charm quark mass, the factorization and renormalization scales and due to uncertainties related to the PDF set used. A more detailed description of how these uncertainties are treated has been discused in section 3.2. FONLL calculations used within this thesis are taken from the web page [20]. By default, fragmentation fractions for a charm quark hadronizing into the considered D meson are set to be one. Therefore, these calculations have been scaled using fragmentation fractions quoted in [21]. These are $f(c \to D^0) = 0.565 \pm 0.032$, $f(c \to D^+) = 0.246 \pm 0.020$ and $f(c \to D^{*+}) = 0.224 \pm 0.028$.

In figure 4.3, FONLL predictions have been compared to measurements of the prompt D^0, D^+ and D^{*+} p_{T}-differential cross sections performed by ALICE in proton-proton collisions at $\sqrt{s} = 7\,\mathrm{TeV}$. In this figure, uncertainties related to the measured data points are the quadratically combined statistical and systematic uncertainties, which have been taken from [4]. The shaded areas are theoretical uncertainties of the FONLL predictions. As we can observe, FONLL predictions describe the p_{T}-differential cross section of prompt D^0, D^+ and D^{*+} integrated over $|y| < 0.5$ as measured by ALICE appropriately, since the measured data points and the FONLL calculations agree within the respective uncertainties. The measured p_{T}-distribution is in general larger than the FONLL predictions for the central parameters. In [15] this has been interpreted as that these deviations may indicate a preference of the data for a value of the charm mass smaller than the central value of $m = 1.5\,\mathrm{GeV}$ as used by FONLL. Note however that these are results only integrated over $|y| < 0.5$, where only approximately 10% of the charm quark is expected to be produced according to FONLL calculations. In order to observe if FONLL predictions describe charm production in the forward rapidity range appropriately as well, we compared FONLL and p_{T}-differential cross sections of D^0, D^+ and D^{*+} integrated over bins in rapidity y for $2.0 < y < 4.5$ as measured by LHCb [6] in the figures 4.4, 4.5 and 4.6. We can observe again, that FONLL predictions for the p_{T} distributions and the measured p_{T} spectra agree within the respective uncertainties. The measured values are again in general larger than the FONLL central values as we have observed it in the comparison of FONLL predictions and ALICE measurements.

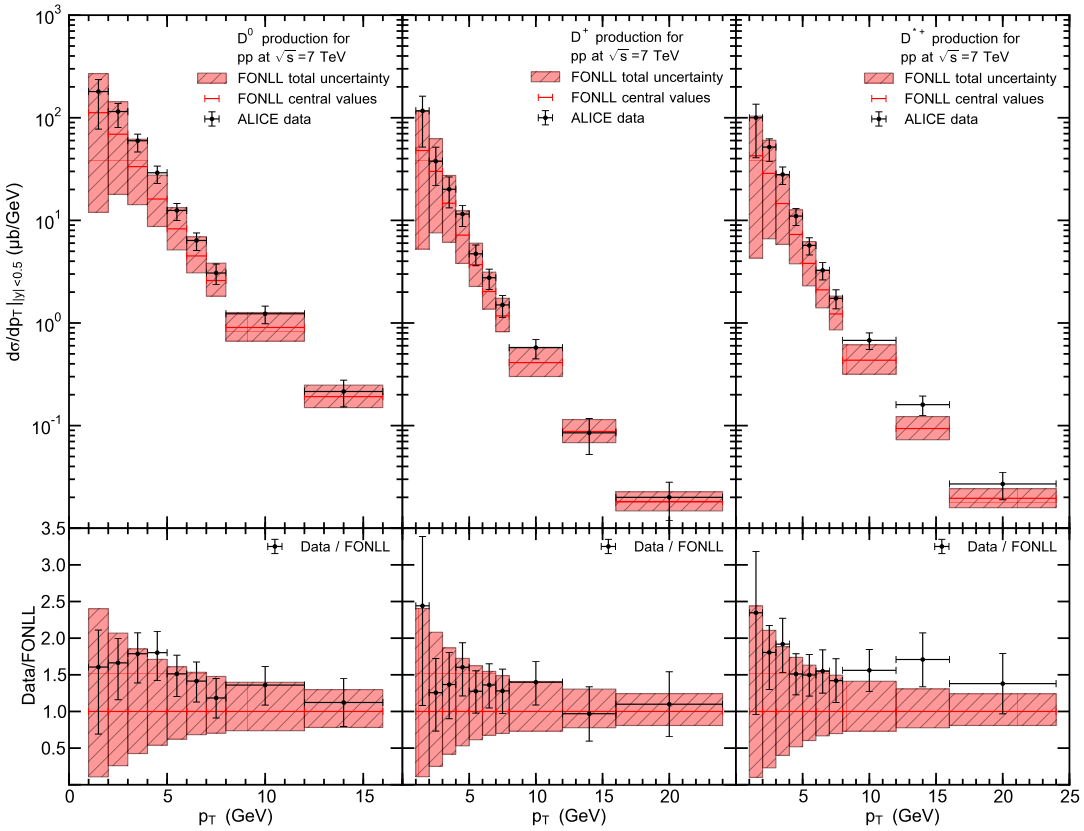

Figure 4.3: Comparison of p_{T}-differential cross sections for prompt D^0, D^+ and D^{*+} production measured by ALICE in proton-proton collisions at $\sqrt{s} = 7\,\mathrm{TeV}$ integrated over the range $|y| < 0.5$ with the corresponding FONLL predictions. The uncertainties of the experimental data include the statistical and systematic uncertainty summed in quadrature. The shaded areas illustrate theoretical uncertainties of the FONLL predictions.

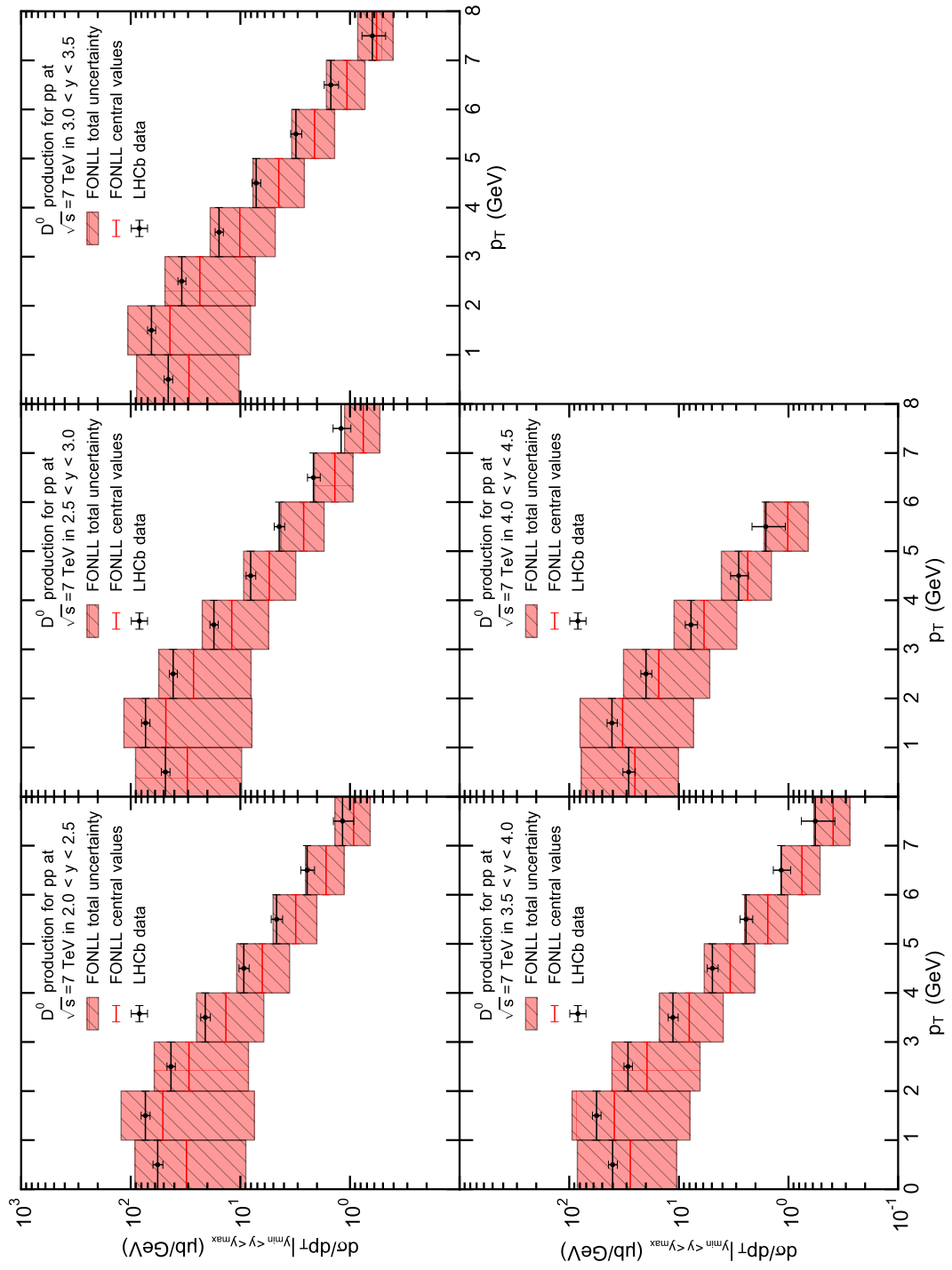

Figure 4.4: Comparison of FONLL predictions and p_{T}-distributions of D^0 measured by LHCb for different ranges in rapidity y.

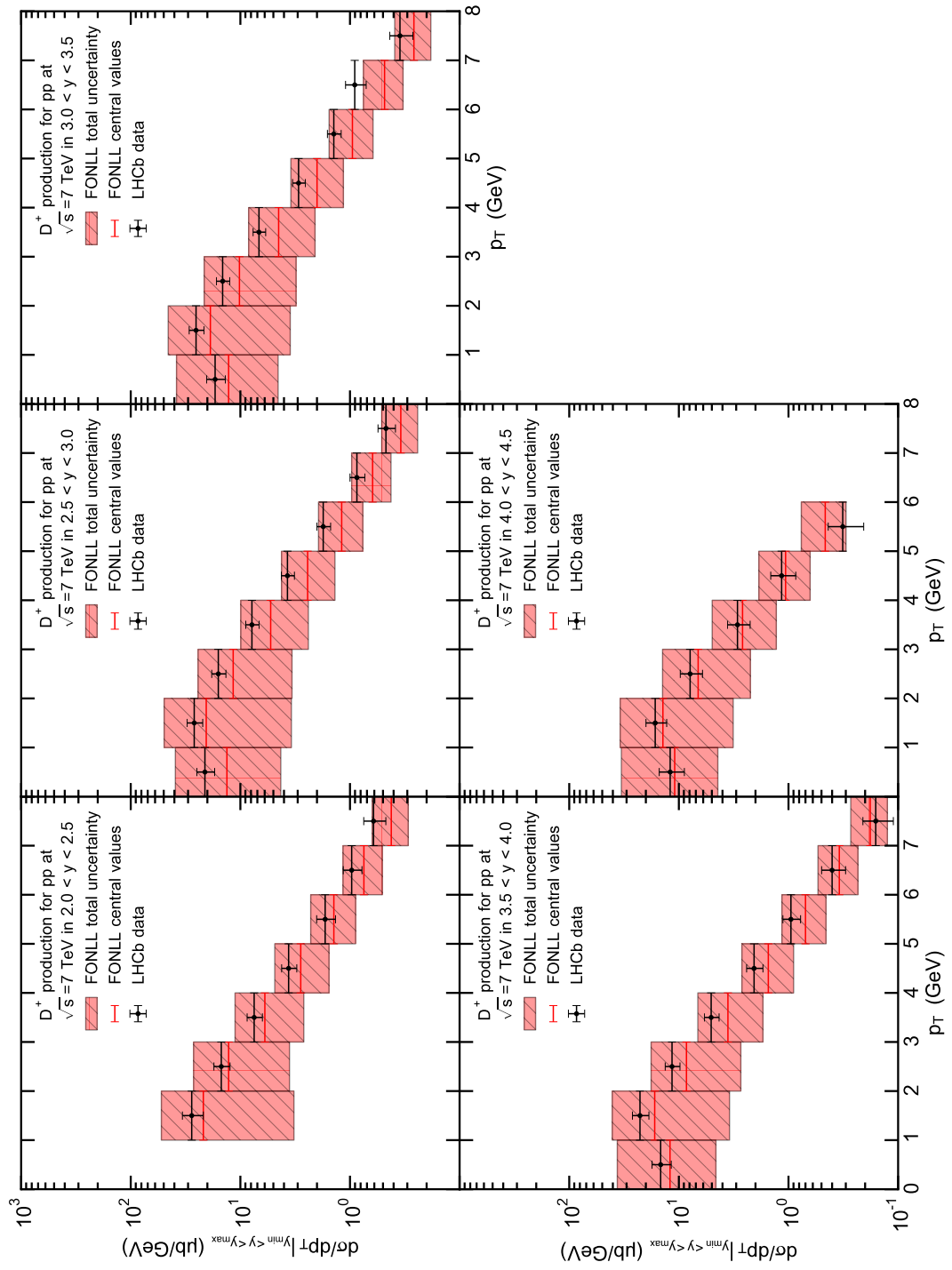

Figure 4.5: Comparison of FONLL predictions and p_{T}-distributions of D^+ measured by LHCb for different ranges in rapidity y.

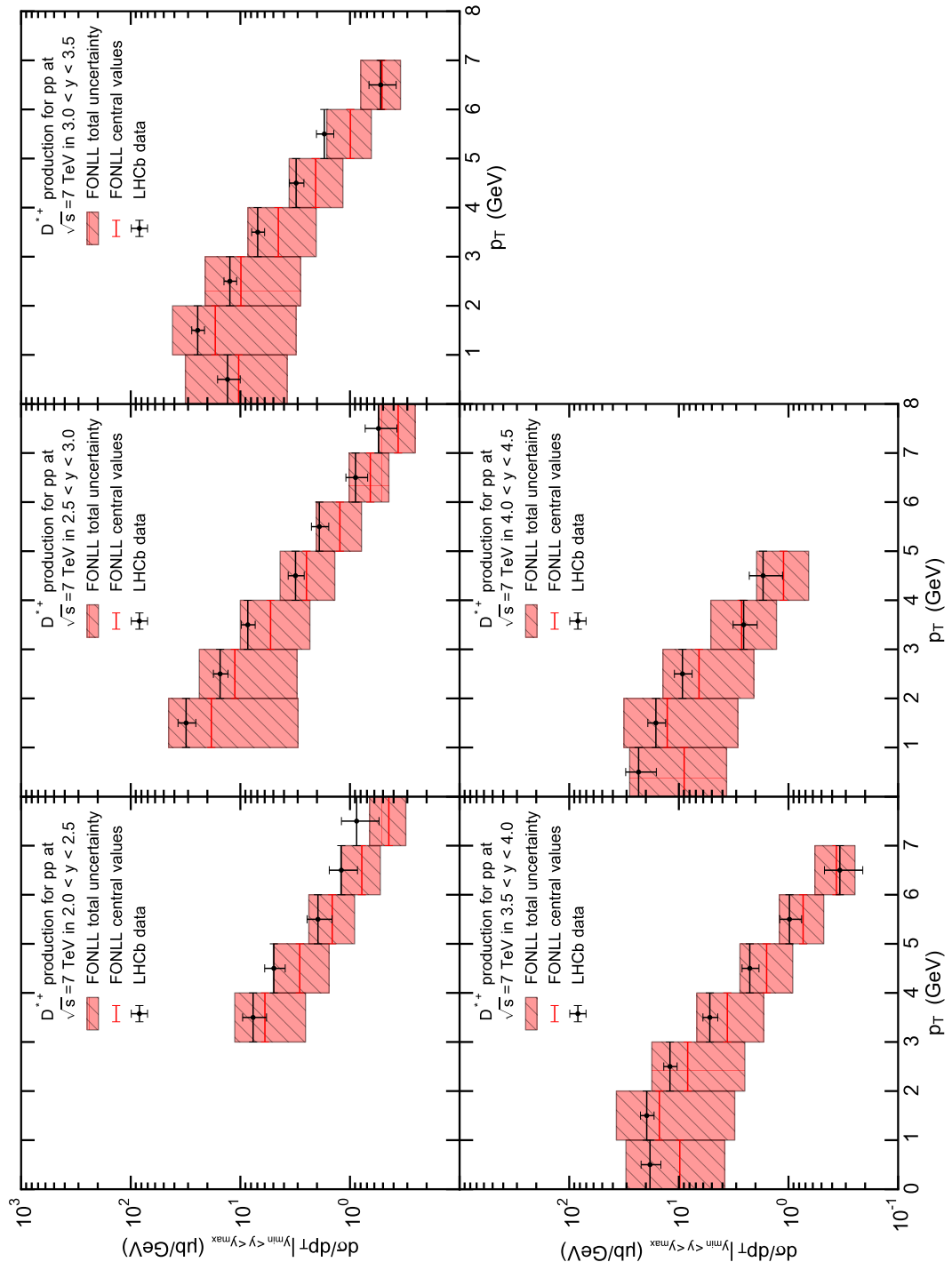

Figure 4.6: Comparison of FONLL predictions and p_{T}-distributions of D^{*+} measured by LHCb for different ranges in rapidity y.

In the end however, the shape of the distributions is described correctly by the FONLL calculations over a large range in rapidity. Therefore we can use FONLL predictions for D^0, D^+ and D^{*+} to extrapolate their cross sections.

For the theoretical prediction of D_s^+, we will adapt a method used in [6]. There, it has been argued, that D_s^+ and D^{*+} are kinematically similar. Therefore, to describe D_s^+ spectra, predictions for D^{*+} have been scaled with $f(c \to D_s^+)/f(c \to D^{*+})$, where $f(c \to D_s^+) = 0.080 \pm 0.017$ [21]. In figure 4.7, FONLL predictions are compared to measurements of the p_{T}-differential cross section of prompt D_s^+ as measured by ALICE [5]. Observing the ratios of the measured points to the central predictions obtained by FONLL we can state, that these can be considered to be constant within the uncertainties. In figure 4.8, the FONLL calculations are compared to data from LHCb [6] measurements for different bins within $2.0 < y < 4.5$. The predictions describe the shape of the measured values within the uncertainties. So, we can use FONLL calculations for D^{*+} with the respective fragmentation fraction to describe the spectra of D_s^+.

To describe prompt Λ_c^+ cross sections we used predictions obtained from the event generator PYTHIA 8.175 [25]. We simulated proton-proton collisions at $\sqrt{s} = 7\,\mathrm{TeV}$ for six different tunes of the generator. For each of these tunes, we generated one million events and selected prompt Λ_c^+. In order to compare the PYTHIA results with measurements of p_{T}-differential cross section by LHCb, we counted the number of selected Λ_c^+ baryons within the range $2.0 < y < 4.5$ and $2\,\mathrm{GeV} < p_{\mathrm{T}} < 8\,\mathrm{GeV}$ for bins in p_{T} of the size $1\,\mathrm{GeV}$. The statistical uncertainty is given as the square root of the number of Λ_c^+ in the respective bin. To obtain p_{T}-differential cross section, the numbers counted have been multiplied by the ratio of the total cross section summed over all allowed processes to the total number of accepted events. The minimal and maximal predictions obtained for different settings of the tune define the theoretical uncertainty of the PYTHIA predictions, which are depicted as shaded areas in figure 4.9. Although we can observe deviations between the LHCb measurements and the PYTHIA predictions, the shape is described correctly since the ratios between the measured data points and the PYTHIA predictions can be considered as being constant. Thus, we can use PYTHIA predictions to extrapolate Λ_c^+ cross sections.

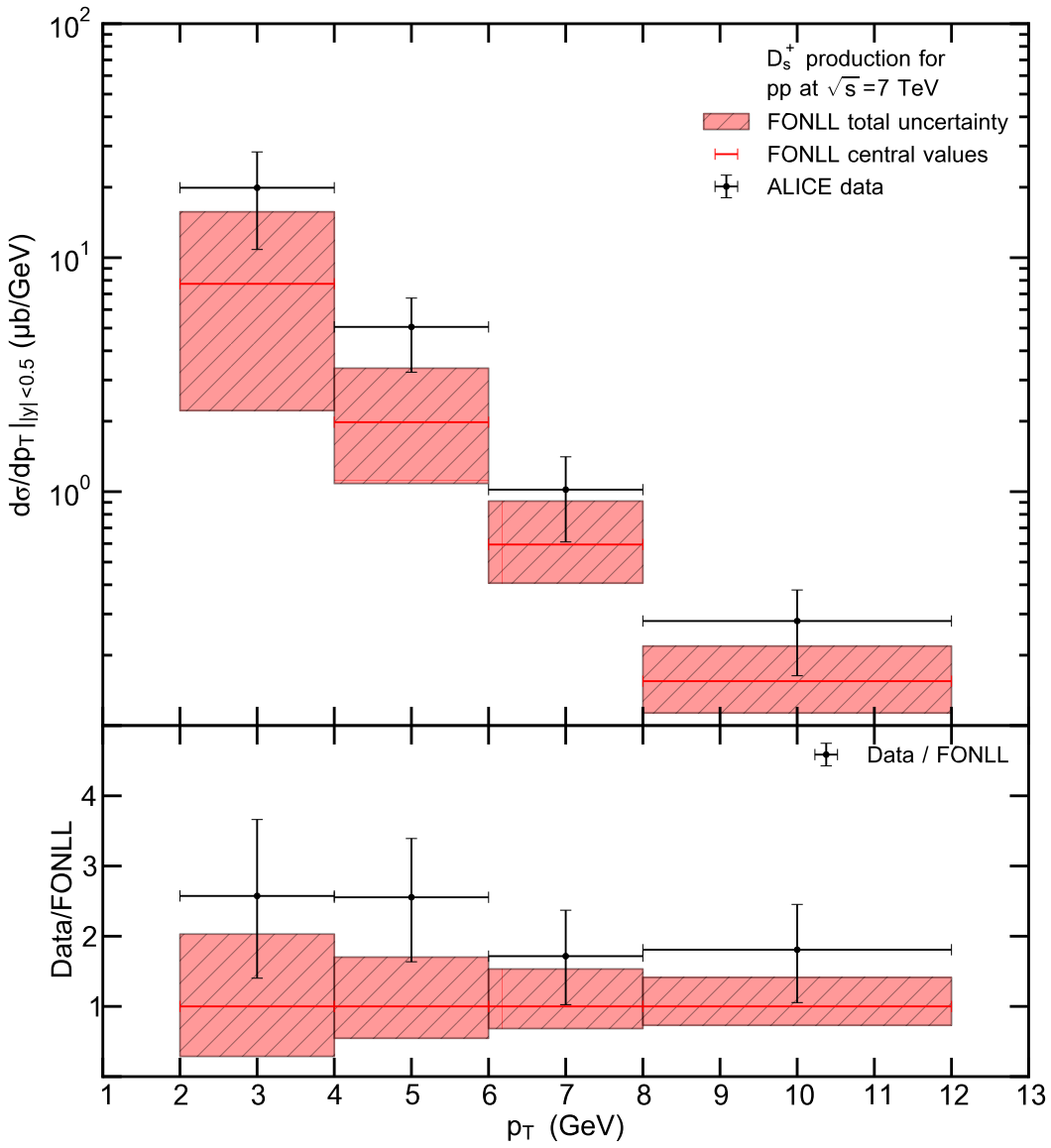

Figure 4.7: Comparison of the p_{T}-distribution of D_s^+ measured by ALICE in the range $|y| < 0.5$ to the FONLL predictions for D^{*+} scaled with $f(c \to D_s^+)/f(c \to D^{*+})$. The uncertainties related to the data points are the quadratically combined statistical and systematic uncertainties provided in [5]. The shaded areas are the uncertainty ranges of the FONLL predictions.

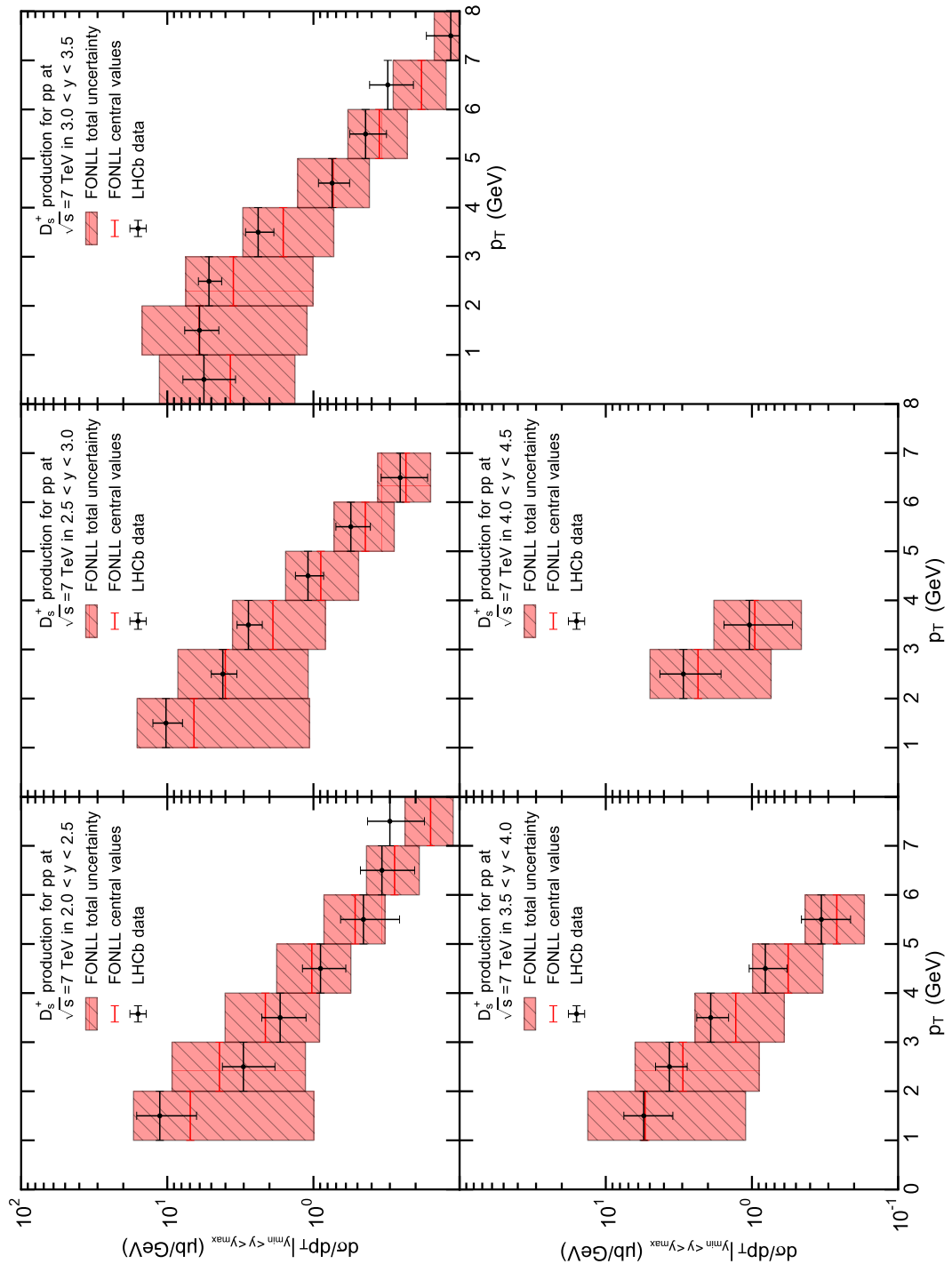

Figure 4.8: Comparison of FONLL predictions and p_{T}-distributions of D_s^+ measured by LHCb for different ranges in rapidity y.

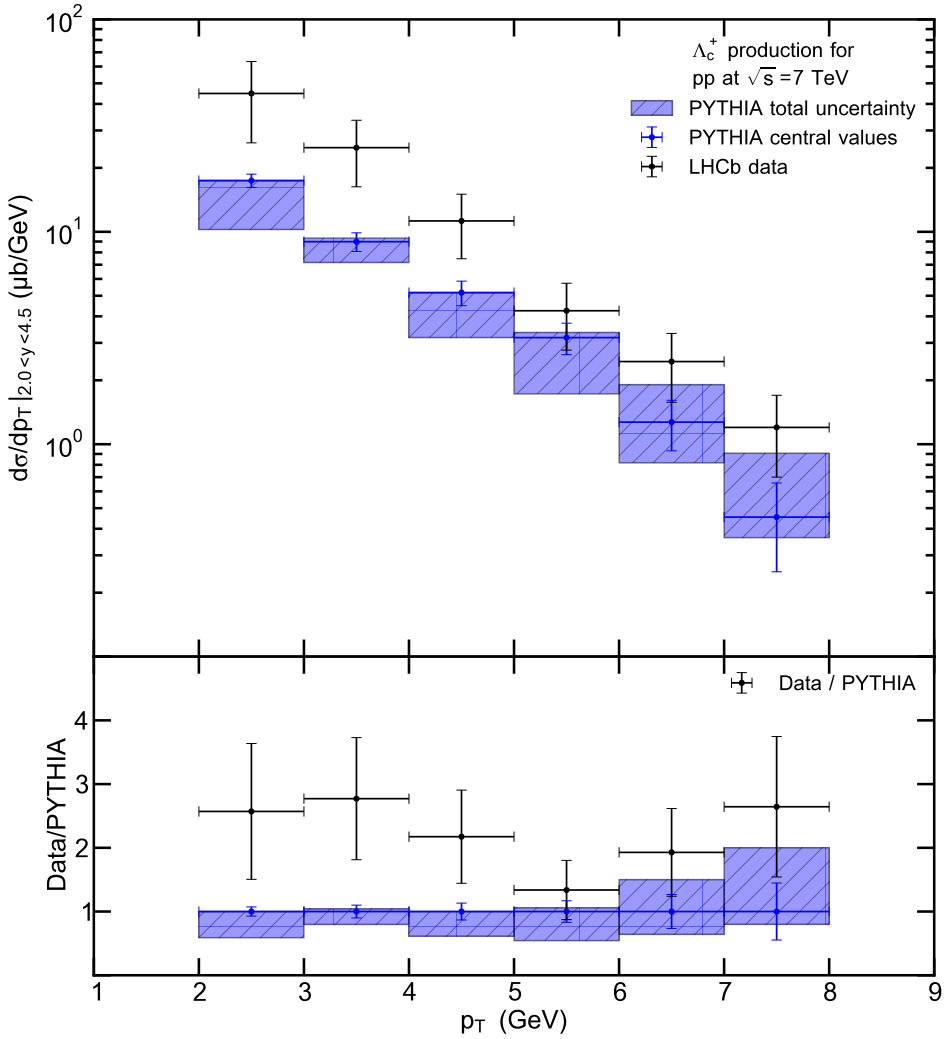

Figure 4.9: Comparison of the p_{T}-distribution of Λ_c^+ measured by LHCb in the range $2.0 < y < 4.5$ to the spectrum obtained from the PYTHIA 8.175 [25] event generator. The uncertainties related to the data points are the quadratically combined statistical and systematic uncertainties provided in [6]. The shaded areas are the uncertainty ranges of the PYTHIA predictions obtained by calculating the cross section for different tunes and then taking the envelop. The central values correspond to the default setting of the tune. The errobars of the PYTHIA calculations are statistical uncertainties of the PYTHIA predictions.

4.4 Extrapolation of charmed hadron cross sections

In this section, we will describe how the cross sections have been extrapolated using predictions from FONLL and PYTHIA and how the uncertainties have been propagated. We have extrapolated the charmed hadron cross sections for the three domains

$$B_1 = \{(p_{\mathrm{T}}, y) \in \mathbb{R}_{\geq 0} \times \mathbb{R}\} \,, \tag{4.31}$$

$$B_2 = \{(p_{\mathrm{T}}, y) \in \mathbb{R}_{\geq 0} \times (-0.9, 0.9)\} \,, \tag{4.32}$$

$$B_1 = \{(p_{\mathrm{T}}, y) \in \mathbb{R}_{\geq 0} \times (2.5, 4.0)\} \tag{4.33}$$

corresponding to the total phase space and the mid and forward rapidity ranges covered by ALICE. We will use these extrapolated cross sections to extrapolate the charm pair cross section.

Extrapolation of D meson cross sections

As already discussed in the previous section 4.3, we will use FONLL predictions to extrapolate D meson cross sections. The different predictions provided by the web-interface [20] have been described in section 3.2. The extrapolated cross section and the uncertainties have been determined as follows.

1. We have calculated the integrated cross sections $\sigma_A^{\mathrm{FONLL}}(D)$ and $\sigma_B^{\mathrm{FONLL}}(D)$ as defined in equation 4.1 and equation 4.2 using the central predictions for the corresponding meson species D. Depending on the D meson, the domain A is one of the domains A_1, A_2, A_3, A_4 defined by the equations 4.21 to 4.24, which describe the regions covered by the combined measurements. B denotes the domain of extrapolation.

2. We have calculated the extrapolation factor corresponding to the central predictions $f_A^B(D) = \sigma_B^{\mathrm{FONLL}}(D)/\sigma_A^{\mathrm{FONLL}}(D)$. The value of the extrapolated cross section is then given by $\sigma_B^{\mathrm{extr}}(D) = \sigma_A^{\mathrm{expr}}(D) \cdot f_A^B(D)$.

3. The combined cross sections $\sigma_A^{\mathrm{expr}}(D)$ have statistical (stat) and systematic (syst) uncertainties as well as uncertainties related to the integrated luminosity (lum) and to the branching ratios (BR) of the analyzed decay channels. These uncertainties have been propagated using Gaussian propagation of uncertainties and the central value of the extrapolation factor $f_A^B(D)$. This means, that the corresponding uncertainties of

the extrapolated cross sections have been obtained by simply scaling them with the central extrapolation factor. That is, we have for the propagated uncertainties

$$\Delta\sigma_B^{\text{extr}}(D) = \Delta\sigma_A^{\text{expr}}(D) \cdot f_A^B(D) \,. \tag{4.34}$$

4. As described in section 3.2, FONLL calculations have theoretical uncertainties which have to be accounted for in our extrapolation procedure. Since these uncertainties affect the extrapolation factor we will call them extrapolation uncertainties (extr). To determine these uncertainties, we use the different predictions listed in section 3.2. So, these uncertainties have been determined in four steps.

   In the first step, we determined variations of the extrapolated cross sections due to variations of the charm quark mass. We used the predictions $(\sigma_A^{\text{FONLL}}(D))_{\texttt{min\_mass}}$, $(\sigma_B^{\text{FONLL}}(D))_{\texttt{min\_mass}}$ and $(\sigma_A^{\text{FONLL}}(D))_{\texttt{max\_mass}}$, $(\sigma_B^{\text{FONLL}}(D))_{\texttt{max\_mass}}$ to determine the corresponding extrapolation factors $(f_A^B(D))_{\texttt{min\_mass}}$, $(f_A^B(D))_{\texttt{max\_mass}}$ and extrapolated cross sections

$$\begin{aligned}(\sigma_B^{\text{extr}}(D))_{\texttt{min\_mass}} &= \sigma_A^{\text{expr}}(D) \cdot (f_A^B(D))_{\texttt{min\_mass}} \\ (\sigma_B^{\text{extr}}(D))_{\texttt{max\_mass}} &= \sigma_A^{\text{expr}}(D) \cdot (f_A^B(D))_{\texttt{max\_mass}}\end{aligned}$$

   The difference between the maximum and minimum of these values and the central prediction is then considered to be the uncertainty due to variation of the mass. Thus, we have

$$(\Delta\sigma_B^{\text{extr}}(D))_{+\text{mass}} = \max\{(\sigma_B^{\text{extr}}(D))_{\texttt{min\_mass}}, (\sigma_B^{\text{extr}}(D))_{\texttt{max\_mass}}\} - \sigma_B^{\text{extr}}(D) \,, \tag{4.35}$$

$$(\Delta\sigma_B^{\text{extr}}(D))_{-\text{mass}} = \sigma_B^{\text{extr}}(D) - \min\{(\sigma_B^{\text{extr}}(D))_{\texttt{min\_mass}}, (\sigma_B^{\text{extr}}(D))_{\texttt{max\_mass}}\} \,. \tag{4.36}$$

   In the second step, we determined the uncertainties related to the PDF accordingly using extrapolated cross sections $(\sigma_B^{\text{extr}}(D))_{\texttt{min\_pdf}}$ and $(\sigma_B^{\text{extr}}(D))_{\texttt{max\_pdf}}$. The uncertainties are then given by

$$(\Delta\sigma_B^{\text{extr}}(D))_{+\text{PDF}} = \max\{(\sigma_B^{\text{extr}}(D))_{\texttt{min\_pdf}}, (\sigma_B^{\text{extr}}(D))_{\texttt{max\_pdf}}\} - \sigma_B^{\text{extr}}(D) \,, \tag{4.37}$$

$$(\Delta\sigma_B^{\text{extr}}(D))_{-\text{PDF}} = \sigma_B^{\text{extr}}(D) - \min\{(\sigma_B^{\text{extr}}(D))_{\texttt{min\_pdf}}, (\sigma_B^{\text{extr}}(D))_{\texttt{max\_pdf}}\} \,. \tag{4.38}$$

   In the third step, the FONLL predictions $(\sigma_A^{\text{FONLL}}(D))_{(\xi_F,\xi_R)}$ and $(\sigma_B^{\text{FONLL}}(D))_{(\xi_F,\xi_R)}$ for the integrated cross sections using different settings of the scales as described in

section 3.2 have been used to obtain a set of extrapolated cross sections

$$(\sigma_B^{\mathrm{extr}}(D))_{(\xi_F,\xi_R)}$$

using equation 4.3. If $\mathcal{S} = \{(0.5, 0.5), (2, 2), (2, 1), (1, 2), (1, 0.5), (0.5, 1)\}$ describes the set of scale settings for ξ_F and ξ_R as given in section 3.2, then the uncertainty of the extrapolated cross section due to variations of the renormalization and factorization scales is given by

$$(\Delta\sigma_B^{\mathrm{extr}}(D))_{+\mathrm{scale}} = \max\{(\sigma_B^{\mathrm{extr}}(D))_{(\xi_F,\xi_R)} \mid (\xi_F, \xi_R) \in \mathcal{S}\} - \sigma_B^{\mathrm{extr}}(D)\ , \tag{4.39}$$

$$(\Delta\sigma_B^{\mathrm{extr}}(D))_{-\mathrm{scale}} = \sigma_B^{\mathrm{extr}}(D) - \min\{(\sigma_B^{\mathrm{extr}}(D))_{(\xi_F,\xi_R)} \mid (\xi_F, \xi_R) \in \mathcal{S}\}\ . \tag{4.40}$$

Finally, the total uncertainty is the quadratic combination of the uncertainties due to mass, PDF and scales variations. This means that the total extrapolation uncertainty is given by

$$(\Delta\sigma_B^{\mathrm{extr}}(D))_{\pm\mathrm{extr}} = \sqrt{(\Delta\sigma_B^{\mathrm{extr}}(D))^2_{\pm\mathrm{mass}} + (\Delta\sigma_B^{\mathrm{extr}}(D))^2_{\pm\mathrm{PDF}} + (\Delta\sigma_B^{\mathrm{extr}}(D))^2_{\pm\mathrm{scale}}}\ .$$

Extrapolation of Λ_c^+ cross section

In the case of the Λ_c^+ baryon we used prediction obtained from the event generator PYTHIA 8.175. We have generated one million events for proton-proton collisions at $\sqrt{s} = 7\,\mathrm{TeV}$ for six different tunes of the event generator. These tunes are denoted as `Tune:pp = 1` to `Tune:pp = 6`. A description of these tunes can be found in the online manual [26]. We will denote these tunes by indices $i \in \{1, 2, \ldots, 6\}$ in the following. The default setting is `Tune:pp = 5`. We will describe step by step how we extrapolated cross sections for Λ_c^+ using PYTHIA predictions.

1. For each tune of the event generator we analyzed one million events. To account only for prompt Λ_c^+, we turned off decays of bottomed hadrons. Detected Λ_c^+ baryons have been selected and properties like the trasverse momentum p_{T} or rapidity y have been stored in separate textfiles.

2. For the default setting of the tune we counted the number $N_A^{\mathrm{PYTHIA}}(\Lambda_c^+)$ of prompt Λ_c^+ within the domain A of the combined measurements and the number $N_B^{\mathrm{PYTHIA}}(\Lambda_c^+)$ within the domain B of the extrapolation.

3. We can consider the counting of prompt Λ_c^+ baryons as a counting experiment. Basically, the extrapolation factor is given by

$$f_A^B(\Lambda_c^+) = N_B^{\mathrm{PYTHIA}}(\Lambda_c^+)/N_A^{\mathrm{PYTHIA}}(\Lambda_c^+) \; .$$

However, since we do not know how $N_A^{\mathrm{PYTHIA}}(\Lambda_c^+)$ and $N_B^{\mathrm{PYTHIA}}(\Lambda_c^+)$ are correlated, we cannot deduce the statistical uncertainty of the extrapolation factor. Therefore, we used a Monte Carlo method to obtain the extrapolation factor with its statistical uncertainty. That is, we drew one million random numbers X_A^k and X_B^k from two Poisson-distribution with the single parameter of the distribution set equal to $N_A^{\mathrm{PYTHIA}}(\Lambda_c^+)$ and $N_B^{\mathrm{PYTHIA}}(\Lambda_c^+)$ respectively. For each drawn pair of random numbers X_A^k and X_B^k we calculated $(f_A^B(\Lambda_c^+))^k = X_B^k(\Lambda_c^+)/X_A^k(\Lambda_c^+)$. The mean of $(f_A^B(\Lambda_c^+))^k$ and its standard deviation are considered to be the value $f_A^B(\Lambda_c^+)$ of the extrapolation factor and its statistical uncertainty. The value of the extrapolated cross section of Λ_c^+ is then given by

$$\sigma_B^{\mathrm{extr}}(\Lambda_c^+) = \sigma_A^{\mathrm{expr}}(\Lambda_c^+) \cdot f_A^B(\Lambda_c^+) \; .$$

4. The statistical uncertainty of the combined experimental cross section $\sigma_A^{\mathrm{expr}}(\Lambda_c^+)$ and the statistical uncertainty of the extrapolation factor $f_A^B(\Lambda_c^+)$ determined in the previous step have been added quadratically giving the statistical uncertainty of the extrapolated cross section. Thus, we have

$$(\Delta\sigma_B^{\mathrm{extr}}(\Lambda_c^+))_{\pm\mathrm{stat}} = \sqrt{\left(\frac{(\Delta\sigma_A^{\mathrm{expr}}(\Lambda_c^+))_{\pm\mathrm{stat}}}{\sigma_A^{\mathrm{expr}}(\Lambda_c^+)}\right)^2 + \left(\frac{(\Delta f_A^B(\Lambda_c^+))_{\pm\mathrm{stat}}}{f_A^B(\Lambda_c^+)}\right)^2} \cdot \sigma_B^{\mathrm{extr}}(\Lambda_c^+) \; .$$

5. The remaining uncertainties of the combined experimental cross section $\sigma_A^{\mathrm{expr}}(\Lambda_c^+)$, that is the systematic uncertainty and the uncertainties related to uncertainties of the integrated luminosity and branching ratio, have been propagated by multiplying them with the extrapolation factor $f_A^B(\Lambda_c^+)$. Thus, we have

$$\Delta\sigma_B^{\mathrm{extr}}(\Lambda_c^+) = \Delta\sigma_A^{\mathrm{expr}}(\Lambda_c^+) \cdot f_A^B(\Lambda_c^+) \; .$$

6. For each tune $i \in \{1, 2, \ldots, 6\}$ the corresponding extrapolation factor $(f_A^B(\Lambda_c^+))_i$ has been determined as described in the third step using Poisson-distributions and the numbers of prompt Λ_c^+ counted for each tune within the respective domains.

For each extrapolation factor $(f_A^B(\Lambda_c^+))_i$ we calculated the extrapolated cross section $(\sigma_B^{\text{extr}}(\Lambda_c^+))_i$. The extrapolation uncertainty is determined as the difference between the maximal and minimal values predicted for the different tunes and the central prediction. So, the extrapolation uncertainty is given by

$$(\Delta\sigma_B^{\text{extr}}(\Lambda_c^+))_{+\text{extr}} = \max\{(\sigma_B^{\text{extr}}(\Lambda_c^+))_i \mid i \in \{1,2,\ldots,6\}\} - \sigma_B^{\text{extr}}(\Lambda_c^+) \,,$$
$$(\Delta\sigma_B^{\text{extr}}(\Lambda_c^+))_{-\text{extr}} = \sigma_B^{\text{extr}}(\Lambda_c^+) - \min\{(\sigma_B^{\text{extr}}(\Lambda_c^+))_i \mid i \in \{1,2,\ldots,6\}\} \,.$$

Extrapolation results for the charmed hadron cross sections

We have written a code to perform the calculations as described above. To check if the code worked correctly, we performed the extrapolation of D^0, D^+ and D^{*+} total cross sections using only the ALICE measurements and compared our extrapolated cross sections to the results cited in [22], which have been extrapolated in the same way. We were able to reproduce the results. After the verification of our code, we extrapolated charmed hadron cross sections. The results of the extrapolation of the charmed hadron cross sections for the different domains of the phase space are summarized in the tables 4.5, 4.6 and 4.7.

Extrapolation of P_{v}

The cross sections of D^+ and D^{*+} have been extrapolated for the total phase space B_1 as explained in the beginning of this section. For the sake of convenience, we will drop the reference to B_1 in the notation and denote these cross sections simply as $\sigma^{\text{extr}}(D^+)$ and $\sigma^{\text{extr}}(D^{*+})$. Using these extrapolated results, we can calculate the ratio P_{v} of $c\bar{d}$ D mesons produced in a vector state to those produced in a vector or pseudoscalar state.

The ratio P_{v} is given by

$$P_{\text{v}} = \frac{N(D^{*+})}{N(D^{*+}) + N(D^+) - N(D^{*+}) \cdot (1 - \mathcal{B}(D^{*+} \to D^0\pi^+))} \,. \tag{4.41}$$

The number of particles is proportional to the cross section. Therefore, we can extrapolate P_{v} using the extrapolated cross sections of the D^+ and D^{*+} mesons. The central

Hadron	$\sigma_{B_1}^{\text{extr}}$	stat.	syst.	lum.	BR	extr.
D^0	4040.8	± 71.2	$^{+242.7}_{-348.8}$	± 116.6	± 52.4	$^{+115.5}_{-70.7}$
D^+	1646.1	± 53.3	$^{+155.4}_{-198.1}$	± 45.7	± 34.5	$^{+105.5}_{-44.8}$
D^{*+}	1719.4	± 72.4	$^{+150.1}_{-209.0}$	± 46.3	± 25.8	$^{+120.4}_{-62.3}$
D_s^+	545.1	± 43.6	$^{+58.4}_{-61.9}$	± 15.1	± 31.4	$^{+125.1}_{-29.2}$
Λ_c^+	894.2	± 105.5	$^{+139.4}_{-139.4}$	± 31.2	± 232.5	$^{+65.7}_{-0.0}$

Table 4.5: Results of the extrapolation for the integrated cross section over the complete phase space. All numbers are given in units of μb.

Hadron	$\sigma_{B_2}^{\text{extr}}$	stat.	syst.	lum.	BR	extr.
D^0	846.4	± 14.9	$^{+50.8}_{-73.1}$	± 24.4	± 11.0	$^{+60.3}_{-175.9}$
D^+	344.8	± 11.2	$^{+32.6}_{-41.5}$	± 9.6	± 7.2	$^{+32.2}_{-64.0}$
D^{*+}	360.2	± 15.2	$^{+31.5}_{-43.8}$	± 9.7	± 5.4	$^{+41.0}_{-66.9}$
D_s^+	114.2	± 9.1	$^{+12.2}_{-13.0}$	± 3.2	± 6.6	$^{+18.8}_{-15.8}$
Λ_c^+	187.9	± 22.9	$^{+29.3}_{-29.3}$	± 6.6	± 48.9	$^{+20.1}_{-2.1}$

Table 4.6: Results of the extrapolation for the integrated cross section over the central rapidity domain $|y| < 0.9$. All numbers are given in units of μb.

Hadron	$\sigma_{B_3}^{\text{extr}}$	stat.	syst.	lum.	BR	extr.
D^0	519.5	± 9.2	$^{+31.2}_{-44.8}$	± 15.0	± 6.7	$^{+44.1}_{-4.1}$
D^+	211.6	± 6.9	$^{+20.0}_{-25.5}$	± 5.9	± 4.4	$^{+25.8}_{-3.5}$
D^{*+}	221.1	± 9.3	$^{+19.3}_{-26.9}$	± 6.0	± 3.3	$^{+28.0}_{-5.3}$
D_s^+	70.1	± 5.6	$^{+7.5}_{-8.0}$	± 1.9	± 4.0	$^{+20.9}_{-3.0}$
Λ_c^+	123.9	± 15.4	$^{+19.3}_{-19.3}$	± 4.3	± 32.2	$^{+0.0}_{-15.7}$

Table 4.7: Results of the extrapolation for the integrated cross section over the forward rapidity range $2.5 < y < 4.0$. All numbers are given in units of μb.

value for the extrapolated P_{v} is given by

$$P_{\mathrm{v}}^{\mathrm{extr}} = \frac{\sigma^{\mathrm{extr}}(D^{*+})}{\sigma^{\mathrm{extr}}(D^{*+}) + \sigma^{\mathrm{extr}}(D^{+}) - \sigma^{\mathrm{extr}}(D^{*+}) \cdot (1 - \mathcal{B}(D^{*+} \to D^{0}\pi^{+}))}$$
$$= \frac{\sigma^{\mathrm{extr}}(D^{*+})}{\sigma^{\mathrm{extr}}(D^{+}) + \sigma^{\mathrm{extr}}(D^{*+}) \cdot \mathcal{B}(D^{*+} \to D^{0}\pi^{+})} \,. \tag{4.42}$$

The uncertainties originating from the measured cross sections have been determined using Gaussian propagation of uncertainties. However, note that there is no uncertainty related to the integrated luminosity since it cancels out in the calculations of P_{v}. The extrapolation uncertainties have been determined as described for the extrapolation of D meson cross sections. That is, we have calculated the ratio P_{v} for all FONLL predictions and obtained uncertainties related to mass variation, uncertainties in the PDF and variations of the scales, which have been added quadratically to determine the total extrapolation uncertainty. Using the extrapolated cross sections in table 4.5, we obtain

$$P_{\mathrm{v}}^{\mathrm{extr}} = 0.612 \pm 0.019\ (\mathrm{stat})^{+0.046}_{-0.061}\ (\mathrm{syst}) \pm 0.009\ (\mathrm{BR})^{+0.007}_{-0.008}\ (\mathrm{extr}) \,.$$

This value is smaller from what we would expect from simple spin counting, that is $P_{\mathrm{v}} = 3/(3+1) = 0.75$ since there are three spin states for D^{*+} and one for D^{+}. This argument originates from heavy-quark effective theory assuming that the difference between the masses of the two D mesons can be neglected for large enough heavy quark masses. In [22] it is noted, that there are also predictions in the range 0.55 to 0.64 within the framework of statistical models. Our extrapolated value is within this range. Further, our result also agrees with the ATLAS value [3]

$$P_{\mathrm{v}}^{\mathrm{ATLAS}} = 0.63 \pm 0.03\ (\mathrm{stat})^{+0.02}_{-0.03}\ (\mathrm{syst}) \pm 0.02\ (\mathrm{BR})^{+0.04}_{-0.02}\ (\mathrm{extr})$$

within uncertainties.

4.5 Extrapolation of charm pair cross section

The charm pair cross section has been determined for the domains B_1, B_2 and B_3 given by the equations 4.31, 4.32 and 4.33. The central value of this cross section is simply given by the sum of the cross sections of D^0, D^+, D_s^+ and Λ_c^+. Note that the cross section of D^{*+} does not contribute to the charm pair cross section, since it decays into

D^0 and D^+. Further, there is a residual part of approximately 1% (see figure 4.1) which has been neglected since we expect the total uncertainties to be significantly larger than this residual contribution to the charm cross section. Therefore, we have

$$\sigma_B^{\text{extr}}(c\bar{c}) = \sigma_B^{\text{extr}}(D^0) + \sigma_B^{\text{extr}}(D^+) + \sigma_B^{\text{extr}}(D_s^+) + \sigma_B^{\text{extr}}(\Lambda_c^+) \,. \tag{4.43}$$

The uncertainties originating from the measurements, that is statistical and systematic uncertainties as well as uncertainties resulting from uncertainties of the integrated luminosity and branching ratios have been propagated using Gaussian propagation of uncertainties. They are given by

$$\Delta\sigma_B^{\text{extr}}(c\bar{c}) = \sqrt{\Delta\sigma_B^{\text{extr}}(D^0)^2 + \Delta\sigma_B^{\text{extr}}(D^+)^2 + \Delta\sigma_B^{\text{extr}}(D_s^+)^2 + \Delta\sigma_B^{\text{extr}}(\Lambda_c^+)^2} \,. \tag{4.44}$$

To determine the extrapolation uncertainty, we have to divide the charm pair cross section into two parts. The first part should only contain FONLL and the second part only PYTHIA predictions. The second part is simply given by the cross section of the Λ_c^+ baryon, since this is the only particle where we used PYTHIA predictions. The FONLL contribution is given by the sum

$$\sigma_B^{\text{extr}}(D^0, D^+, D_s^+) = \sigma_B^{\text{extr}}(D^0) + \sigma_B^{\text{extr}}(D^+) + \sigma_B^{\text{extr}}(D_s^+) \,. \tag{4.45}$$

To obtain the extrapolation uncertainty of this expression, we have calcualted the set of extrapolated values

$$(\sigma_B^{\text{extr}}(D^0, D^+, D_s^+))_i = (\sigma_B^{\text{extr}}(D^0))_i + (\sigma_B^{\text{extr}}(D^+))_i + (\sigma_B^{\text{extr}}(D_s^+))_i \,, \tag{4.46}$$

with $(\sigma_B^{\text{extr}}(D))_i = \sigma_A^{\text{expr}}(D) \cdot (f_A^B(D))_i$. For convenience, we used an index i to denotes the values obtained for different settings of the FONLL parameters as described in section 3.2. The extrapolation uncertainty of $\sigma_B^{\text{extr}}(D^0, D^+, D_s^+)$ is then calculated by determining the mass, the scales and the PDF contributions and adding them in quadrature. For the final result of the extrapolation uncertainty, we have also accounted for the extrapolation uncertainty of the PYTHIA contribution. Therefore, the extrapolation uncertainty of the charm pair cross section is given by

$$(\Delta\sigma_B^{\text{extr}}(c\bar{c}))_{\pm\text{extr}} = \sqrt{(\Delta\sigma_B^{\text{extr}}(D^0, D^+, D_s^+))^2_{\pm\text{extr}} + (\Delta\sigma_B^{\text{extr}}(\Lambda_c^+))^2_{\pm\text{extr}}} \,. \tag{4.47}$$

The charm pair cross section has been extrapolated for the three different domains B_1, B_2 and B_3 corresponding to the total phase space, the mid rapidity range $|y| < 0.9$ and the forward rapidity domain $2.5 < y < 4.0$. The results are summarized in table 4.8.

Domain	$\sigma_B^{\mathrm{extr}}(c\bar{c})$	stat.	syst.	lum.	BR	extr.	total
B_1 (total)	7126.2	± 144.7	$^{+325.4}_{-429.1}$	± 129.9	± 242.9	$^{+350.2}_{-122.9}$	$^{+570.4}_{-544.1}$
B_2 (mid)	1493.3	± 30.9	$^{+68.2}_{-89.9}$	± 27.2	± 51.0	$^{+112.4}_{-247.7}$	$^{+146.9}_{-271.6}$
B_3 (forward)	925.1	± 20.0	$^{+42.5}_{-55.6}$	± 16.8	± 33.5	$^{+90.7}_{-18.4}$	$^{+108.8}_{-72.4}$

Table 4.8: Extrapolation results for the charm pair cross section in different domains of the phase space. B_1 denotes the total phase space, B_2 the central rapidity domain $|y| < 0.9$ and B_3 the forward range $2.5 < y < 4.0$. All numbers are given in units of μb.

In figure 4.10 we compare our extrapolated cross section for the total phase space to total cross sections provided by LHCb in [27], by ATLAS in [3] and by ALICE in [22]. The uncertainties given in that figure are the total uncertainties, which have been determined by adding all individual contributions to the uncertainty quadratically. We can observe that our determined value for the total charm pair cross section agrees with the other values within uncertainties. However, our value has a much smaller total uncertainty than the other values being of approximately 8%. So we can conclude, that combining the measurements of ALICE and LHCb enabled us to reduce the extrapolation uncertainty, which was the dominant contribution to the total uncertainty. Figure 4.11 shows the energy dependence of the total nucleon-nucleon charm pair cross section. The values correspond to different experiments and are given in [3], [22], [27], [28], [29] and [30]. These results are compared to NLO calculations [31]. We can observe, that all values are within the uncertainty band of the NLO calculations. However, they are all above the central prediction illustrated by the continuous line. This possibly indicates that the charm quark mass is less than assumed in the NLO calculation, which is 1.5 GeV for the central predictions. This is further supported by a recent analysis of cross sections in deep inelastic electron-positron scattering at HERA, which extracts a charm mass $m_c = 1.26 \pm 0.06\,\mathrm{GeV}$ [32] where the given uncertainty is the quadratic combination of the single contributions.

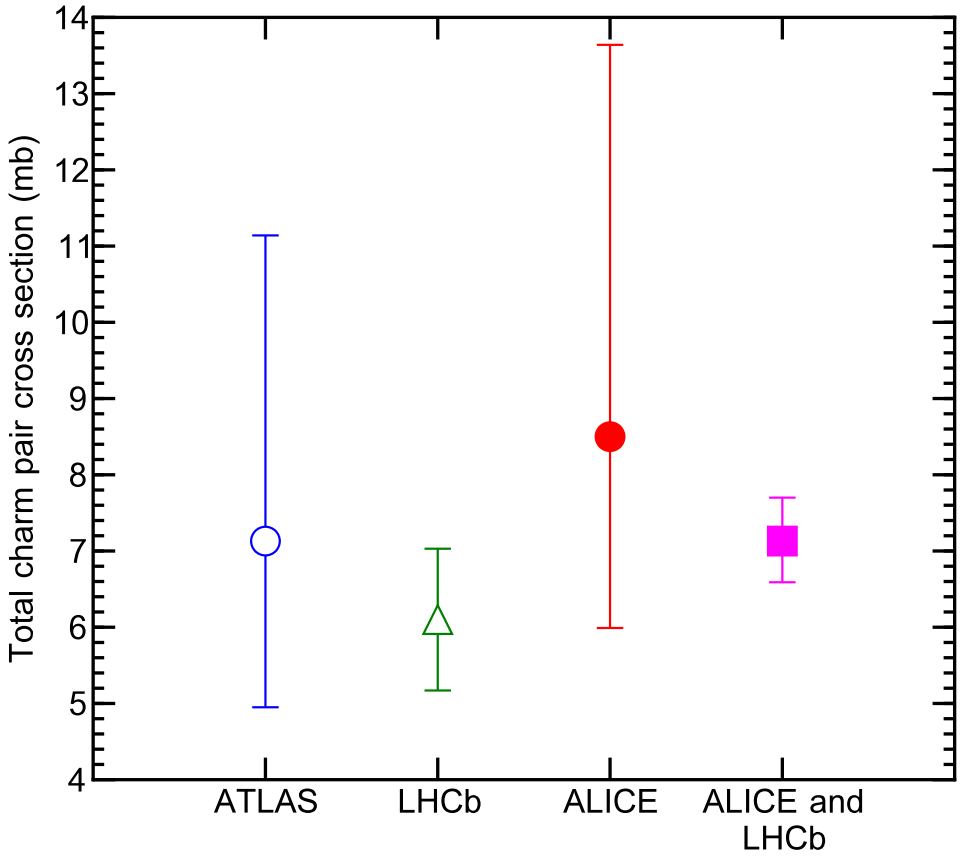

Figure 4.10: Comparison of our extrapolated cross section for the total phase space to total cross sections provided by LHCb in [27], by ATLAS in [3] and by ALICE in [22].

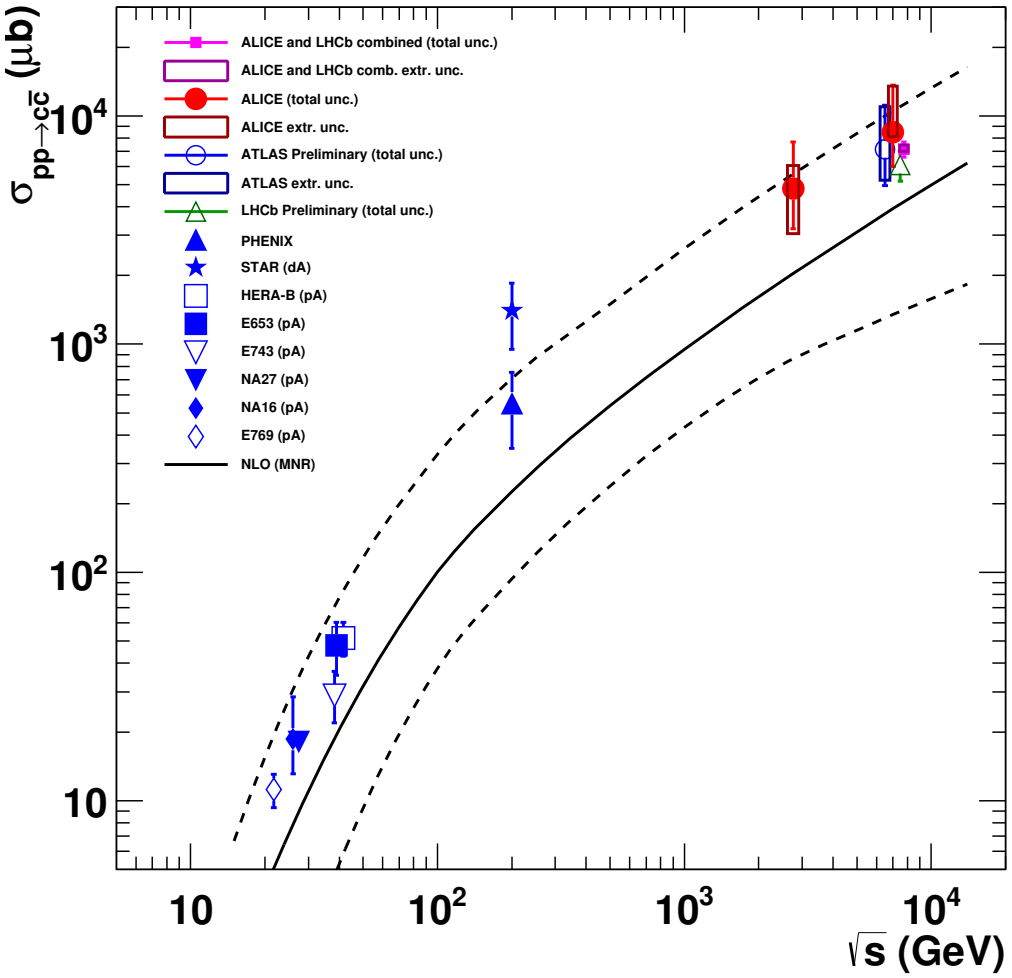

Figure 4.11: The energy dependence of the total charm pair cross section. The values are from [3], [22], [27], [28], [29] and [30]. In case of proton-nucleus (pA) or deuteron-nucleus (dA) collisions, the measured cross sections have been scaled down by the number of binary nucleon-nucleon collisions calculated in a Glauber model of the proton-nucleus or deuteron-nucleus collision geometry [22]. The results are compared to NLO calculations [31].

5 Summary

Within this thesis the total charm pair production cross section in proton-proton collisions at $\sqrt{s} = 7\,\text{TeV}$ was determined. We compared predictions for the p_T-distributions obtained from the FONLL framework with experimental data measured by ALICE and LHCb. We observed, that FONLL predictions were appropriate to describe the shape of the spectra. Since FONLL prediction are only available for D mesons, we compared Λ_c^+ data with predictions obtained from the event generator PYTHIA 8.175. We observed again, that the shape of the p_T-spectrum is well described by the PYTHIA predictions. Therefore, we decided to use FONLL predictions to extrapolate D meson and PYTHIA predictions to extrapolate Λ_c^+ cross sections. In order to take advantage of the ALICE and LHCb measurements, we combined these cross section covering a large domain of the (p_T, y) phase space. We were able to reduce the relative extrapolation uncertainty of the total charm pair cross section being now approximately 5%:

$$\sigma_\text{tot}(c\bar{c}) = 7.13 \pm 0.14\ (\text{stat})^{+0.33}_{-0.43}\ (\text{syst}) \pm 0.13\ (\text{lum}) \pm 0.24\ (\text{BR})^{+0.35}_{-0.12}\ (\text{extr})\,\text{mb}\ ,$$

$$\sigma_\text{tot}(c\bar{c}) = 7.13^{+0.57}_{-0.54}\ (\text{total})\,\text{mb}\ .$$

The relative total uncertainty is approximately 8%. Compared to former results provided in [3], [22] and [27] this is an improvement of a factor of two for the relative uncertainty and thus the most precise determination of the total charm pair production cross section at the LHC so far.

References

[1] P. Braun-Munzinger, K. Redlich, J. Stachel, *Particle Production in Heavy Ion Collisions*, Invited review for Quark Gluon Plasma 3, eds. R. C. Hwa and Xin-Nian Wang (World Scientific Publishing) 491, arXiv:nucl-th/0304013.

[2] A. Andronic, P. Braun-Munzinger, K. Redlich, J. Stachel, *The statistical model in Pb-Pb collisions at the LHC*, Nucl. Phys. A904-905 2013, 535c (2013), arXiv:1210.7724 [nucl-th].

[3] ATLAS Coll., ATLAS-PHYS-PUB-2011-012 (2011), ATLAS-CONF-PUB-2011-017 (2011).

[4] ALICE Coll., CERN-PH-EP-2011-181, arXiv:1111.1553v2 [hep-ex].

[5] ALICE Coll., CERN-PH-EP-2012-227, arXiv:1208.1948v2 [hep-ex].

[6] LHCb Coll., CERN-PH-EP-2013-009, arXiv:1302.2864 [hep-ex].

[7] J. D. Hunter, *Matplotlib: A 2D graphics environment*, Computing In Science & Engineering volume 9 number 3, pages 90–95, IEEE COMPUTER SOC, 2007.

[8] J. Beringer *et al.* (Particle Data Group), *Review of Particle Physics*, Phys. Rev. D86, 010001 (2012).

[9] J. C. Collins, D. E. Soper and G. Sterman, *Perturbative QCD*, Singapore, World Scientific, 1989.

[10] P. Nason, S. Dawson and R. K. Ellis, *The Total Cross Section for the Production of Heavy Quarks in Hadronic Collisions*, Nucl. Phys. **B303** (1988) 607.

[11] P. Nason, S. Dawson and R. K. Ellis, *The one Particle inclusive Differential Cross Section for Heavy Quark Production in Hadronic Collisions*, Nucl. Phys. **B327** (1989) 49, *Erratum*, Nucl. Phys. **B335** (1990) 260.

[12] M. Cacciari, *Large $p_\perp$ Hadroproduction of Heavy Quarks*, arXiv:hep-ph/9311260.

[13] M. Cacciari, M. Greco and P. Nason, *The p_T spectrum in heavy-flavour hadroproduction*, JHEP **9805** (1998) 007, arXiv:hep-ph/9803400.

[14] M. Cacciari, P. Nason and C. Oleari, *A Study of Heavy Flavoured Meson Fragmentation Functions in e^+e^- annihilation*, JHEP **0605** (2006) 006, arXiv:hep-ph/0510032.

[15] M. Cacciari, S. Frixione and P. Nason, *The p_T spectrum in heavy-flavor photoproduction*, JHEP **0103** (2001) 006, arXiv:hep-ph/0102134.

[16] M. Cacciari, P. Nason, *Charm Cross Section for the Tevatron Run II*, JHEP **0309** (2003) 006, arXiv:hep-ph/0306212.

[17] E. Braaten, K. Cheung, S. Flemming and T. C. Yuan, *Perturbative QCD Fragmentation Functions as a Model for Heavy-Quark Fragmentation*, Phys. Rev. D **51** (1995) 4819, arXiv:hep-ph/9409316.

[18] P. M. Nadolsky *et. al*, *Implications of CTEQ gloabal analysis for collider observables*, Phys. Rev. D **78** (2008) 013004, arXiv:0802.0007 [hep-ph].

[19] P. M. Nadolsky, Z. Sullivan, *PDF uncertainties in WH production at Tevatron*, arXiv:hep-ph/0110378.

[20] `http://www.lpthe.jussieu.fr/~cacciari/fonll/fonllform.html` (23.06.2013)

[21] Particle Data Group, C. Amsler *et al.*, *Fragmentation functions in e^+e^- annihilation and lepton-nucleon DIS*, in *Review of Particle Physics*, Phys. Lett. **B667** (2008).

[22] ALICE Coll., CERN-PH-EP-2012-133, arXiv:1205.4007v2 [hep-ex].

[23] LHCb Coll., LHCb-ANA-2011-018, CERN-LHCb-ANA-2011-018 (2011).

[24] R. J. Barlow, *Asymmetric Systematic Errors*, arXiv:physics/0306138.

[25] T. Sjöstrand, S. Mrenna and P. Skands, JHEP05 (2006) 026, Comput. Phys. Comm. 178 (2008) 852.

[26] `http://home.thep.lu.se/~torbjorn/pythia81php/Welcome.php` (23.06.2013)

[27] LHCb Coll., LHCb-CONF-2010-013 (2010).

[28] C. Lorenço, H. K. Wöhri, Phys. Rept. **433** 127 (2006).

[29] STAR Coll., Phys. Rev. D **85** 092010 (2012), arXiv:1204.4244 [nucl-ex].

[30] PHENIX Coll., Phys. Rev. C **84** 044905 (2011).

[31] M. Mangano, P. Nason, G. Ridolfi, Nucl. Phys. **B 373** 295 (1992).

[32] H1 Collaboration, ZEUS Collaboration, *Combination and QCD Analysis of Charm Production Cross Section Measurements in Deep-Inelastic ep Scattering at HERA*, arXiv:1211.1182 [hep-ex].

Acknowledgements

First of all, I would like to express my gratitude to Dr. Kai Schweda, who has been my tutor in the particle physics course *Experimentalphysik V* and who has been my supervisor for this thesis. He supported me when I needed help and his guidance helped me to overcome challenges I faced in writing this thesis.

During the work on my thesis I had the oppurtunity to attend the group meetings of the ALICE group at the Physikalisches Institut and to present my results. Their critism and ideas helped me improving my thesis. Therefore, I would like to express my gratitude to the group as well.

Jochen Klein helped me to get the event generator PYTHIA going. He also answered some of my questions regarding the theoretical background of the heavy quark production. Yifei Wang read the theoretical part of my thesis and we had valuable discussions on the FONLL framework. Many thanks for their help.

I would like to thank Francesca Dordei from the LHCb group, who provided me parts of the internal analysis notes for the charm production measurements in which the integrated cross sections of the LHCb measurements with their uncertainties were given.

Many thanks go also to M. Cacciari, who provided FONLL calculations, vital for the extrapolation of the charm pair cross section, on a publicly accessible web page.

This work has been supported by the Federal Ministry of Education and Research under promotional reference 06HD197D and by the Helmholtz Alliance HA216/EMMI.

Erklärung

Ich versichere, dass ich diese Arbeit selbstständig verfasst und keine anderen als die angegebenen Quellen und Hilfsmittel benutzt habe.

Heidelberg, den 12.07.2013